

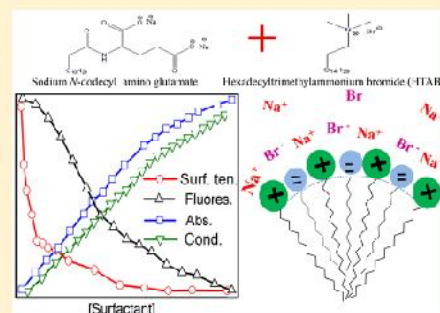
REPRINTS

Interfacial and Aggregation Behavior of Dicarboxylic Amino Acid-Based Surfactants in Combination with a Cationic Surfactant

Manas Barai,[†] Manas Kumar Mandal,[†] Atanu Karak,[†] Romain Bordes,^{*,‡,§} Anuttam Patra,^{*,§} Sudipta Dalai,[†] and Amiya Kumar Panda^{*,†,§}[†]Department of Chemistry and Chemical Technology, Vidyasagar University, Midnapore 721102, West Bengal, India[‡]Chemistry and Chemical Engineering, Applied Surface Chemistry, Chalmers University of Technology, SE-412 96 Gothenburg, Sweden[§]Chemistry of Interfaces Group, Luleå University of Technology, SE-97187 Luleå, Sweden

Supporting Information

ABSTRACT: The interfacial and micellization behavior of three dicarboxylic amino acid-based anionic surfactants, abbreviated as AAS (N-dodecyl derivative of -aminomalonnate, -aspartate, and -glutamate) in combination with hexadecyltrimethylammonium bromide (HTAB) were investigated by surface tension, conductance, UV–vis absorption/emission spectroscopy, dynamic light scattering (DLS), and viscosity studies. Critical micelle concentration (CMC) values of the surfactant mixtures are significantly lower than the predicted values, indicating associative interaction between the components. Surface excess, limiting molecular area, surface pressure at the CMC, and Gibbs free energy indicate spontaneity of the micellization processes compared to the pure components. CMC values were also determined from the sigmoidal variation in the plot of micellar polarity and pyrene UV–vis absorption/emission intensities with surfactant concentration. The aggregation number, determined by static fluorescence quenching method, increases with decreasing mole fraction of the AAS (α_{AAS}), where the micelles are mainly dominated by the HTAB molecules. The size of the micelle increases with decreasing α_{AAS} , leading to the formation of larger and complex aggregates, as also supported by the viscosity studies. Micelles comprising 20–40 mol % AAS are highly viscous, in consonance with their sizes. Some of the mixed surfactant systems show unusual viscosity (shear thickening and increased viscosity with increasing temperature). Such mixed surfactant systems are considered to have potential in gel-based drug delivery and nanoparticle synthesis.



INTRODUCTION

The self-aggregation behavior of a mixed surfactant system depends on its composition and environmental conditions such as temperature, pressure, salinity, and solvent nature.^{1–4} They usually have lower CMCs than the individual components because of specific attractive/associative interactions.^{5–9} A series of systematic investigations have been carried out by Kumar et al. using a number of different oppositely charged binary surfactant/amphiphile mixtures where strong synergistic interactions between the oppositely charged components were observed.^{6–9} Different kinds of interactions such as adhesive/cohesive forces and hydrogen bonding, operative for such systems, result in the lower CMC values.¹⁰ Studies on different mixed surfactants include cationic/anionic,¹¹ cationic/cationic,¹² cationic/nonionic,¹³ anionic/nonionic,¹⁴ and zwitterionic/anionic¹⁵ systems, to mention a few. Oppositely charged surfactant mixtures, through electrostatic attraction, form a variety of aggregates depending on the chain length of an individual surfactant.^{1,3,16–23} An equimolar mixture of oppositely charged

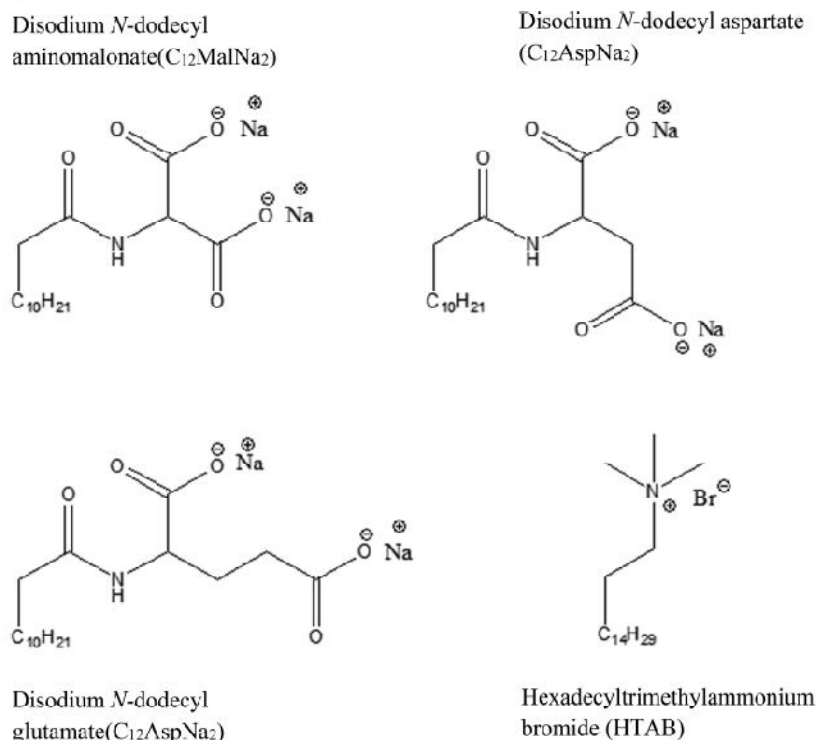
surfactants in an aqueous medium forms an ion pair amphiphile (IPA), also known as a coacervate, because it quite often precipitates out.^{3,18,19,24–28} An IPA usually contains two hydrocarbon chains; the two alkyl chains are non-covalently attached, whereby electrostatic interaction occurs between the oppositely charged headgroups,²⁴ which facilitates precipitation/coacervation. Electrostatic interactions between the two oppositely charged surfactant headgroups result in different hydration energy of the surfactant mixtures compared to that of the individual surfactant.^{18,19,24–26,28} Oppositely charged mixed surfactant systems can achieve a higher surface activity and a lower CMC compared to the surfactant components.^{6–9,19} Studies involving bivalent anionic surfactants, for example, the presently investigated N-dodecyl derivatives of -aminomalonnate, -aspartate, and -glutamate (AASs), in combination with a cationic surfactant HTAB are

Received: September 16, 2019

Revised: October 23, 2019

Published: November 5, 2019

Scheme 1. Chemical Structures of the Surfactants



not common in the literature. Oppositely charged mixed surfactants mainly form micelles and vesicles in aqueous media; the dianionic groups are dominant factors in regulating this unique aggregation behavior.¹⁷ With a slight excess of either of the surfactants, it is quite common to experience the formation of vesicles.^{17,29–32} The surface ionic charge from the excess surfactant is shielded/screened by two factors: (i) charge neutralization and (ii) the presence of excess salt, produced from the counterions of the two surfactants.³⁰ In the case of a cationic–anionic mixed surfactant system, the micellar aggregation number is very high because such systems can form stable vesicles without the need for high energy methods such as sonication and extrusion.³³ In general, surfactant mixtures can form various complex phases.³⁴ Precipitation, coacervation,³⁵ and liquid crystal formation³⁶ arise at extremely low surfactant concentration. The appearance of different phases or liquid crystals in the case of mixed surfactants sturdily depends on the composition, number of alkyl chains per surfactant, temperature, and salinity.⁴ It is expected that the presently studied oppositely charged mixed surfactant systems would exhibit associative electrostatic interaction through the surfactant headgroups,^{37,38} thus minimizing the need for individual surfactant components. Conventional single-tailed anionic surfactants (e.g., sodium dodecyl sulfate (SDS) and sodium deoxycholate (NaDC)) have limitations because they can break the C- and N-terminal peptide bonds that prevent DNA translocation, unlike the AASs.³⁹ HTAB exhibits considerable toxicity, which can be significantly reduced by combining it with AASs, where it is expected that the individual toxicities/intolerances could be substantially minimized. Higher-hydrophilicity AASs are significantly different from the corresponding amino acids. Thus, the influence of chain length on the aggregation behavior

of such surfactants in combination with HTAB is considered to be important.

The present study endeavors to investigate the relatively more complex systems: the formation of binary aggregates between amino acid-based surfactants ($C_{12}\text{MalNa}_2$, $C_{12}\text{AspNa}_2$, and $C_{12}\text{GluNa}_2$) and cationic surfactant HTAB. HTAB is well known for its multifaceted applications such as the fabrication of nanomaterials,⁴⁰ drug delivery,⁴¹ cell lysis,⁴² microemulsion formulation,⁴³ molecular separation,⁴⁴ lubrication,⁴⁵ and cleaning operations,⁴⁶ to mention a few. AASs are capable of forming vesicles, for which they show manifold applications in biological systems (e.g., emulsification,⁴⁷ foaming control, surfactant-based separation, surface wetting modification, and flotation⁴⁸).

Another point of interest in the current system is the structural heterogeneity between the two types of surfactants. The AASs have one dodecyl chain while HTAB comprises a hexadecyl chain. The second difference between the AASs and HTAB occurs in terms of the charge on the surfactant headgroups. Because of the difference in the alkyl chain length as well as the smaller charge density in the headgroups of the AASs, the presently investigated systems are less likely to form precipitate at stoichiometric ratios, as is quite common in other conventional binary surfactant mixtures.¹⁴ Most importantly, anionic surfactants *N*-dodecyl aminomalonate, -aspartate, and -glutamate contain two carboxylic acid moieties which are progressively separated by methylene group(s). Thus, it is expected that the structural differences will lead to asymmetry, which in turn would produce complex assemblies. This could have profound effects on the viscosity of the aggregates.

The interfacial behavior and micellar aggregation behavior of mixed surfactants were investigated with different experimental techniques such as surface tension, electrical conductance,

UV–vis absorption/emission spectroscopy, DLS, and viscosity measurements. Different physicochemical parameters (*viz.*, CMC, surface excess (Γ_{\max}), surface pressure at the CMC (π_{CMC}), minimum area of the surfactant molecules at the air–water interface (A_{\min}), Gibbs free energy of micellization (ΔG_m°), interfacial adsorption ($\Delta G_{\text{ads}}^\circ$), fraction of counterion binding (β), hydrodynamic diameter (d_h), polydispersity index (PDI), aggregation number (n), and zero shear viscosity (η^0) values) were evaluated. The influence of counterion specificity is vital for the surface activity of an amphiphile. Dicarboxylic AASs are potential chelating agents for divalent cations. Two carboxylate groups can come in close contact with each other while the adjacent amide bond can also exhibit the metal chelating property.⁴⁹ AASs are not only environmentally benign but also display different specific characteristics of carboxylic polar headgroups.

Until now, no comprehensive studies on mixed surfactants that include the AASs as one of the components have been available in literature. Because AASs contain two anionic carboxylic acid groups, they do not interact prominently with the HTAB because during hydration the polar headgroups of AASs interact with water molecule, so AASs alone cannot be considered to be a suitable candidate for the formation of micelles, where low CMC values are warranted. It is believed that the studies on the interfacial and aggregation behavior of such binary surfactants can provide new insights that will eventually help in understanding the bulk and interfacial activities of mixed surfactant systems.

EXPERIMENTAL SECTION

Materials. HTAB, hexadecylpyridinium chloride (HPC), and pyrene were products from Sigma-Aldrich Chemicals Pvt. Ltd. (USA). Sodium hydroxide was purchased from Fluka (Germany). AASs were synthesized and purified by the previously described method.^{50,51} The purity of the synthesized surfactants was found to be more than 98.5%, and they were used for further studies. Doubly distilled water with a specific conductance of 2–4 μS at 298 K was used throughout the experiments. All of the chemicals were stated to be $\geq 99\%$ pure and were used as received. Structures of HTAB and the newly synthesized surfactants are shown in Scheme 1.

METHODS

Determination of CMC. CMC values of the pure and mixed surfactants were determined by combined surface tension, conductance, and UV–vis absorption/emission spectroscopic techniques.

Surface Tension Studies. Twenty-fold (anticipated or literature value of the CMC) concentrated surfactant solutions were used as stock solutions for performing the conductance study. At first, 20 mL of water was taken in a double-walled jacketed container at a controlled temperature (298 K). The temperature of the container was controlled by an external water circulation bath (Hahntech Corporation, South Korea). A quantitative amount of surfactant stock solution was then progressively added to water. It was then homogenized using a magnetic stirrer. After 3 min of equilibration, the surface tension of the solution was recorded with a du Noüy tensiometer with an accuracy of 0.1 mN m^{-1} (Jencon, Kolkata, India). From the break point of the surface tension (γ) vs $\log C$ plot, the CMC value was determined.

Conductance Studies. A protocol similar to that adopted in the surface tension measurement was followed for the conductance studies, where the conductance of the solution was recorded by a direct reading conductivity meter, a Cyber Scan CON510 (Eutech Instruments, Singapore) with an accuracy of $\pm 0.1 \mu\text{S cm}^{-1}$. The electrode is stated to be a dip-type conductance cell with automatic temperature compensation (ATC) that minimizes the air bubble entrapment during measurement. An electrode with a cell constant of

0.92 cm^{-1} was used. From the break point of the conductance (κ) vs C plots, the CMC values were determined.⁵²

UV–vis Absorption and Emission Spectroscopic Studies. Pyrene was used as the probe for the UV–visible absorption and emission spectroscopic studies. Initially, a 1000 μM pyrene solution was prepared in ethanol, and then it was further diluted to 100 μM using ethanol. A 2.0 μM pyrene (Py) solution in water was obtained by proper dilution and sonication for half an hour. Though the medium contained 0.5% (v/v) alcohol, it was considered to have little effect on the surfactant aggregation. Finally, the 2 μM pyrene solution–dispersion in water was within the solubility limit.¹⁹ UV–vis absorption spectra were recorded with a UV–vis spectrophotometer (UVD-2950, Labomed Inc., USA). Pyrene exhibits three major absorption peaks at 242, 275, and 338 nm and four weak bands at 233, 253, 265, and 322 nm (Figure S1, supplementary section).⁵³ Fluorescence spectroscopic studies were performed with a spectrofluorometer (Hitachi High Technologies Fluorescence Spectrophotometer Corporation, F-7100, Tokyo, Japan), where the first vibronic peak at 373 nm (I_1) and the third vibronic peak at 393 nm (I_3) were considered. Emission spectra of pyrene in the presence of varying surfactant concentration are shown in Figure S1 (supplementary section), along with its absorption spectra. A 4-fold concentrated (compared to the anticipated/reported CMC of surfactant) surfactant solution was used as stock for UV–vis absorption and emission spectroscopic studies. An aqueous pyrene solution (2 mL) was taken in a quartz cuvette, and another cuvette filled with water was used as the reference. A quantitative amount of surfactant solution, prepared in 2 μM pyrene, was progressively added into the experimental cuvette and was homogenized. Absorption spectra were recorded in the wavelength range of 230 to 350 nm. The sum total of the absorbance of all of the major peaks/bands of pyrene (A_T) was plotted against C . From the sigmoidal plot, the CMC value was determined using the following expression⁵⁴

$$T = \frac{(a_i - a_f)}{[1 + \exp^{(x-x_0)/\Delta x}]} + a_f \quad (1)$$

where a_i and a_f are the initial and final asymptotes of the sigmoid, respectively, x_0 is the center of the sigmoid (herein the CMC), and Δx is the interval of the independent variable x . The excitation wavelength of pyrene was set at 335 nm, and the emission spectra were recorded in the wavelength range of 350 to 550 nm. The CMC value was also determined from the sigmoidal curve of the I_1/I_3 vs [surfactant] plot. The micellar aggregation number (n) was determined by the fluorescence quenching method using pyrene as the probe and HPC as the quencher.⁵⁵

DLS studies. d_h and PDI values of the micellar aggregates were measured using a Zetasizer Nano ZS-90 (Malvern Instruments, U.K.) dynamic light scattering spectrometer. Solutions were filtered carefully through a 0.45 μm Millipore cellulose acetate membrane filter. A He–Ne laser operating at 632.8 nm was used as the light source; the scattering angle was set at 90°. A surfactant solution with concentration 10-fold higher than the corresponding CMC values was used for the DLS studies. Solution of higher concentration were highly viscous, which interfered with the DLS studies, so they were avoided.

Viscosity Studies. Viscosity was measured with a DV II-Pro rotoviscometer (Brookfield, USA) with a stated accuracy of ± 0.01 cP. Some surfactant mixtures are highly viscous; they form different liquid crystals (as observed through a polarization optical microscope, data not shown). A 1.0 mL surfactant solution (of different concentrations: 50–150 mM) was taken in the cone-and-plate-type rotoviscometer. The viscosity of pure as well as surfactant mixtures was measured at different shear rates (ranging from 76 to 380 s^{-1}). η^0 was obtained from the intercept of the plot of viscosity vs shear rate by fitting polynomial regression. Experiments were carried out in the temperature range of 288 to 318 K, where the temperature was controlled by a circulating water bath (Hahntech Corporation, South Korea).

All experiments, unless otherwise stated, were carried out at 298 K.

RESULTS AND DISCUSSION

Critical Micelle Concentration (CMC). Representative surface tension (γ) vs $\log C$, specific conductance (κ) vs C , A_T vs C , and I_1/I_3 (ratio of the first and third vibronic emission peaks of pyrene) vs C plots are shown in Figure 1, from which

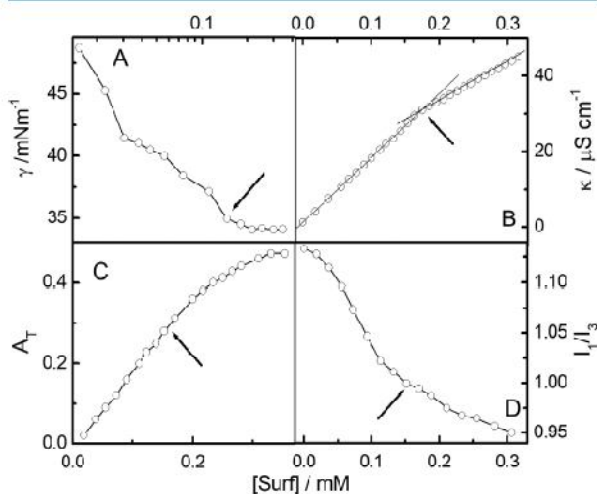


Figure 1. Variation of surface tension (γ), specific conductance (κ), sum of the peak absorbance (A_T), and I_1/I_3 ratio with C at 298 K. A 4:1 (M/M) $C_{12}GluNa_2/HTAB$ mixed surfactant system was used. [Pyrene] = $2 \mu M$. Excitation wavelength = 335 nm.

the CMC value was determined. The CMC of pure HTAB is 0.73 mM, close to the literature value.¹⁹ The CMCs of

$C_{12}MalNa_2$, $C_{12}AspNa_2$, and $C_{12}GluNa_2$ are 51.2, 46.3, and 36.45 mM, respectively, and are also comparable to the literature values.^{50,51} The results are summarized in Table 1. With increasing α_{AAS} , the CMC values gradually increases from the initial lower value of HTAB, indicating an associative interaction between the components that follows the order $C_{12}MalNa_2 + HTAB > C_{12}AspNa_2 + HTAB > C_{12}GluNa_2 + HTAB$ (Figure S2, supplementary section). The CMC values of the mixed surfactants at different mole fractions of the AASs were also calculated theoretically using the Clint formalism (data not shown),^{6,56} and it has been found that the CMC of the surfactant mixtures show significant negative deviation from the theoretically calculated values, which further supports the electrostatic associative interaction between the two oppositely charged surfactants.^{6–9,19} CMC values of pure AASs are higher, and the dianionic carboxylate groups of AAS closely interact with HTAB and can achieve lower CMCs. Variation of the CMC with the surfactant composition will be further discussed in detail in the subsequent section.

Interfacial Behavior. The surface excess (Γ_{max}) of pure and mixed surfactants was calculated according to the Gibbs formalism⁵⁵

$$\Gamma_{max} = -\frac{1}{2.303iRT} \frac{d\gamma}{d \log C} \quad (2)$$

where C represents the surfactant concentration, i is the Gibbs prefactor, and R and T have their usual significances. Γ_{max} is expressed in mol m^{-2} . $i = 3$ is used for the anionic surfactants, and $i = 2$ is used for the cationic surfactant. In the case of mixed surfactant systems, the i values are calculated on the

Table 1. Experimental CMC, Surface Pressure at the CMC (π_{CMC}), Surface Excess (Γ_{max}), Area Minimum (A_{min}), Gibbs Free Energy of Micellization (ΔG_m°), Gibbs Energy Change in Interfacial Adsorption (ΔG_{ads}°), Fraction of Counter Ion Binding (β), and Aggregation Number (n) of the AASs-HTAB Mixed Surfactant System at 298 K

α_{AAS}	CMC/mM						$\pi_{CMC}/\text{mN m}^{-1}$	$10^6 \Gamma_{max}/\text{mol m}^{-2}$	A_{min}/nm^2	molecule^{-1}	$(-\Delta G_m^\circ)/\text{kJ mol}^{-1}$	$(-\Delta G_{ads}^\circ)/\text{kJ mol}^{-1}$	$\beta = (1 - S_2/S_1)$	n
	surface tension	conductivity	fluorescence spectroscopy	UV-vis average	vis average	(CMC _{av})								
HTAB-malonate														
1.0	44.82	50.87	53.85	55.12	51.20	34.4	1.86	0.88	27.59	66.88	0.52	37		
0.8	0.15	0.15	0.16	0.12	0.15	40.9	1.68	0.98	43.68	68.88	0.35	32		
0.6	0.07	0.09	0.10	0.08	0.09	40.9	1.67	0.99	41.47	67.54	0.23	48		
0.5	0.06	0.06	0.11	0.06	0.07	42.2	1.85	0.89	46.68	68.33	0.37	50		
0.4	0.05	0.05	0.08	0.04	0.06	43.1	1.52	1.09	53.24	81.57	0.53	55		
0.2	0.04	0.04	0.05	0.03	0.04	41.5	1.57	1.05	55.45	81.87	0.58	63		
0.0	0.72	0.73	0.75	0.72	0.73	32.6	0.90	1.84	49.58	85.81	0.77	65		
HTAB-aspartate														
1.0	54.18	46.83	41.23	42.87	46.30	32.4	2.38	0.69	26.53	62.36	0.55	51		
0.8	0.15	0.13	0.14	0.14	0.14	39.4	1.75	0.94	41.65	64.18	0.33	28		
0.6	0.09	0.08	0.07	0.08	0.08	39.8	1.83	0.90	42.95	64.19	0.31	32		
0.5	0.04	0.05	0.08	0.07	0.06	40.6	1.70	0.97	46.73	69.52	0.40	48		
0.4	0.04	0.05	0.04	0.06	0.05	41.6	1.38	1.20	47.29	75.71	0.39	54		
0.2	0.04	0.04	0.04	0.03	0.04	40.2	1.39	1.18	55.74	84.39	0.60	62		
HTAB-glutamate														
1.0	33.81	36.67	40.28	35.03	36.45	31.2	2.30	0.71	28.12	56.81	0.60	49		
0.8	0.18	0.16	0.07	0.09	0.12	37.5	1.50	1.07	41.43	66.22	0.28	32		
0.6	0.06	0.08	0.06	0.07	0.07	39.6	1.72	0.96	45.83	69.98	0.35	35		
0.5	0.05	0.06	0.04	0.05	0.05	39.5	1.59	1.04	46.48	71.36	0.35	44		
0.4	0.04	0.05	0.04	0.04	0.04	40.3	1.30	1.27	59.00	90.04	0.60	48		
0.2	0.03	0.04	0.03	0.03	0.03	39.2	1.27	1.30	57.71	88.61	0.65	56		

basis of the relative proportion of surfactants at different mole %. AAS homologues and its mixtures with HTAB are less surface-active than HTAB. The hydrophobicity of AAS homologues is in accordance with its molecular weight, as also reflected through the Γ_{\max} values. Incorporation of the methylene group in between the two carboxylate anions would increase the hydrophobicity of the AASs. Γ_{\max} vs α_{AAS} profiles are shown in Figure 2A.

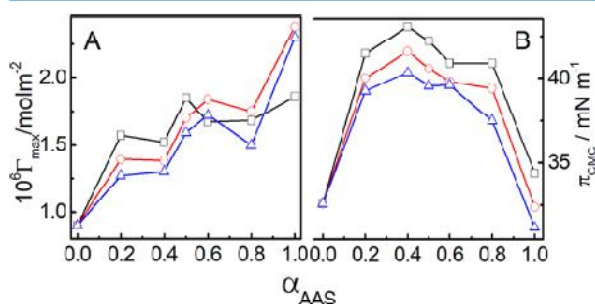


Figure 2. Variation of surface excess (Γ_{\max}) and surface pressure at the CMC (π_{CMC}) with α_{AAS} at 298 K. Systems: \square , $\text{C}_{12}\text{MalNa}_2\text{-HTAB}$; \circ , $\text{C}_{12}\text{AspNa}_2\text{-HTAB}$; and Δ , $\text{C}_{12}\text{GluNa}_2\text{-HTAB}$.

The minimum area per surfactant molecule (A_{\min}) is another parameter that can be evaluated as¹⁹

$$A_{\min} = \frac{10^{21}}{N_A \Gamma_{\max}} \quad (3)$$

where N_A is Avogadro's number. Surface pressure at CMC (π_{CMC}) values were calculated from the surface tension difference between pure water (γ_0) and the surfactant solution at its CMC (γ_{CMC}). The π_{CMC} value of HTAB is 32.6 mN m^{-1} ; for $\text{C}_{12}\text{MalNa}_2$, $\text{C}_{12}\text{AspNa}_2$, and $\text{C}_{12}\text{GluNa}_2$, they are 34.4 , 32.4 , and 31.2 mN m^{-1} , respectively, as shown in Figure 2B. With increasing α_{AAS} the π_{CMC} values gradually decrease and pass through minima because of the higher hydrophobic interaction between the oppositely charged surfactants. For all of the mixed surfactant systems, π_{CMC} values are in the range of 37.5 to 43.1 mN m^{-1} (Table 1). The π_{CMC} values depend on the CMC of the different surfactant mixtures. Two carboxylate anions of $\text{C}_{12}\text{MalNa}_2$ closely interact with HTAB in micelles compared to $\text{C}_{12}\text{AspNa}_2$ and $\text{C}_{12}\text{GluNa}_2$, hence π_{CMC} values follow the sequence $\text{C}_{12}\text{MalNa}_2\text{-HTAB} > \text{C}_{12}\text{AspNa}_2\text{-HTAB} > \text{C}_{12}\text{GluNa}_2\text{-HTAB}$. Γ_{\max} values increase with increasing α_{AAS} . Γ_{\max} of the HTAB molecule is 0.9 mol m^{-2} . For $\text{C}_{12}\text{MalNa}_2$, $\text{C}_{12}\text{AspNa}_2$, and $\text{C}_{12}\text{GluNa}_2$, the Γ_{\max} values are 1.86 , 2.38 , and 2.3 mol m^{-2} , respectively (Table 1). All of the values are close to the literature values.^{50,51} A_{\min} values of AASs are lower than those of HTAB, thus for the mixed surfactants it is expected to decrease with the increasing proportion of AASs. Higher-hydrophilicity AASs molecules prefer to reside in the bulk water rather than at the interface, compared to HTAB. The carboxylate groups get progressively separated through the methylene group(s), thus while moving from $\text{C}_{12}\text{MalNa}_2$ to $\text{C}_{12}\text{AspNa}_2$ to $\text{C}_{12}\text{GluNa}_2$, the spacing between the two polar headgroups increases by one carbon atom sequentially, which leads to the increase in the hydrophobicity of the surfactants.

In consonance with the increasing hydrophobicity, the A_{\min} values follow the sequence $\text{C}_{12}\text{MalNa}_2 > \text{C}_{12}\text{AspNa}_2 > \text{C}_{12}\text{GluNa}_2$. The higher A_{\min} value of the $\text{C}_{12}\text{MalNa}_2\text{-HTAB}$ system implies the formation of a less-packed aggregate

structure. Consequently, Γ_{\max} values decrease and A_{\min} values increase with the increase in α_{AAS} values.

Conductance Studies. CMC values were also determined from the break point of the specific conductance (κ) vs [surfactant] plot as shown in panel B of Figure 1. The degree of counterion dissociation (α) was calculated using the following equation⁵²

$$\alpha = S_2/S_1 \quad (4)$$

where S_1 and S_2 are the slopes of the pre- and postmicellar regions in the specific conductance (κ) vs C plot, respectively. The variation of α with α_{AAS} is graphically shown in panel A of Figure 3. The α value of HTAB is 0.23 ,¹³ whereas for

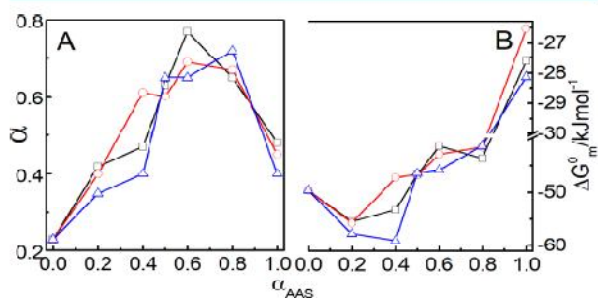
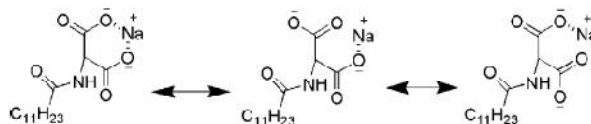


Figure 3. Variation of the degree of dissociation (α) and Gibbs free energy of micellization (ΔG_m^0) with α_{AAS} at 298 K. Systems: \square , $\text{C}_{12}\text{MalNa}_2\text{-HTAB}$; \circ , $\text{C}_{12}\text{AspNa}_2\text{-HTAB}$, and Δ , $\text{C}_{12}\text{GluNa}_2\text{-HTAB}$.

$\text{C}_{12}\text{MalNa}_2$, $\text{C}_{12}\text{AspNa}_2$, and $\text{C}_{12}\text{GluNa}_2$, they are 0.48 , 0.45 , and 0.40 , respectively, close to the previously reported values.^{50,51} AAS molecules remain in more dissociated form than HTAB because of two carboxylate anions; the first dissociation takes away one sodium ion that remains in solution as a free ion. The second sodium ion coordinates with both of the carboxylate anions, stabilizing them, which eventually promotes higher monodissociation of the AASs.



For the $\text{C}_{12}\text{MalNa}_2 + \text{HTAB}$ mixture, with increasing mole % of $\text{C}_{12}\text{MalNa}_2$, α values gradually increase from 0.42 to 0.65 . With increasing α_{AAS} , charge density increases on the micellar surface for which the α value gradually increases, which is also subsequently higher. For the AASs + HTAB mixture, with increasing α_{AAS} , α values pass through maxima because of charge neutralization.

Thermodynamics of Micellization. The change in the Gibbs free energy of micellization (ΔG_m^0) was calculated as⁵²

$$\Delta G_m^0 = (2 - \alpha)RT \ln x_{\text{CMC}} \quad (5)$$

where α is the fraction of counterion dissociation and x_{CMC} is the CMC on the mole fraction scale. R and T have their usual meaning. The Gibbs free energy of interfacial adsorption (ΔG_{ads}^0) was calculated as⁵²

$$\Delta G_{\text{ads}}^0 = \Delta G_m^0 - \frac{\pi_{\text{CMC}}}{\Gamma_{\max}} = \Delta G_m^c - \frac{N_A \pi_{\text{CMC}}}{A_{\min}} \quad (6)$$

The negative value of ΔG_m° ($-49.58 \text{ kJ mol}^{-1}$) for HTAB is close to the literature value,⁵² which indicates its spontaneity of micellization. For $C_{12}\text{MalNa}_2$ -HTAB mixtures, with decreasing mole fraction of $C_{12}\text{MalNa}_2$ (α_{Mal}), the ΔG_m° values become, in general, more negative (-27.59 to $-49.58 \text{ kJ mol}^{-1}$), indicating further spontaneity of micellization and $\Delta G_{\text{acs}}^\circ$ (-61.88 to $-85.81 \text{ kJ mol}^{-1}$). The results are summarized in Table 1 along with other data. The magnitude of the negative ΔG_m° values of AAS-HTAB mixtures decreases from -55.74 to $-26.53 \text{ kJ mol}^{-1}$ for aspartate and from -57.71 to $-28.12 \text{ kJ mol}^{-1}$ for glutamate systems with increasing α_{AAS} as shown in Figure 3B. It is also noted from conductance data that with increasing α_{AAS} , the maximum number of surfactant molecules is dissociated, thus the polarity of the medium increases. In the case of mixed micelles, charge neutralization occurs among the oppositely charged surfactants, and the free counterions further increase the polarity of the medium, which makes the micellization process more favorable.

Micellar Aggregation Number. The micellar aggregation number (n) was calculated using the following equation¹⁹

$$\ln \frac{I_0}{I} = \frac{n[Q]}{[S] - \text{CMC}} \quad (7)$$

where I_0 and I represent the fluorescence intensities of the probe in the absence and presence of quencher (Q, HPC), respectively. $[Q]$ is the quencher concentration, and $[S]$ is the total surfactant concentration. The third vibronic emission peak of pyrene (393 nm) was considered in determining the aggregation number (n). $\ln \frac{I_0}{I}$ vs quencher concentration ($[Q]$) plots are shown in Figure S3 (supplementary section). The aggregation number of HTAB is 65, comparable to the literature value,¹³ whereas for $C_{12}\text{MalNa}_2$, $C_{12}\text{AspNa}_2$, and $C_{12}\text{GluNa}_2$ they are 37, 51, and 49, respectively. The results are shown Table 1 along with other data. For pure as well as mixed surfactant systems, experimentally observed aggregation numbers are in accordance with the micellar composition. With increasing α_{AAS} , n values gradually decrease. The hydrophobicity of HTAB is relatively higher than that of AASs because of its longer hydrocarbon chain length. Besides, while comparing the aggregation numbers of HTAB and the AASs, it has been observed that the aggregation number of HTAB is higher than that of AASs, hence it is quite rational to consider that there will be a greater proportion of HTAB in the mixed micelles. Mixed micelles contain larger proportions of HTAB molecules, hence HTAB mainly dominates the micellar aggregation. In continuation of the present work, considering the experimental values as well as the theoretical values of the CMC of the surfactant mixtures, a number of different formalisms were adopted in analyzing the micellar composition and other parameters.⁶ The theoretical perspectives have been communicated as a separate publication, where it is observed that HTAB always has a larger population than the AASs in the mixed micelles. The hydrophobic interaction and accumulative cross-sectional area of mixed surfactant systems are the main driving forces for the formation of larger and more complex aggregates. Two anionic carboxylate groups of AASs repel each other, which eventually results in the formation of larger aggregates. DLS studies also show that the size of the aggregates increases, further supporting the increased aggregation number for the mixed surfactant systems.

DLS Studies. d_h and PDI values of surfactant aggregates were determined by DLS studies. The d_h of the HTAB

molecule is 1.2 nm, close to the literature value.¹⁹ d_h values of $C_{12}\text{MalNa}_2$, $C_{12}\text{AspNa}_2$, and $C_{12}\text{GluNa}_2$ are 2.2, 2.8, and 3.6 nm, respectively, as shown in Figure 4A. Initially, one of the

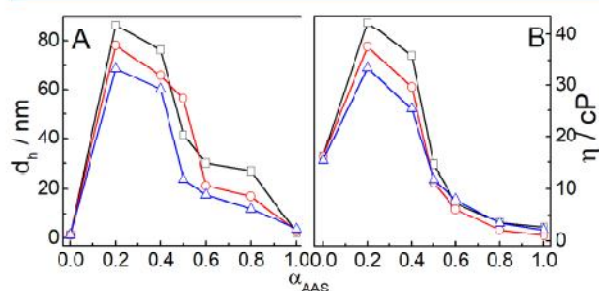


Figure 4. Variation of d_h and viscosity (η) with α_{AAS} at 298 K. Systems: \square , $C_{12}\text{MalNa}_2$ -HTAB; \circ , $C_{12}\text{AspNa}_2$ -HTAB; and Δ , $C_{12}\text{GluNa}_2$ -HTAB.

two carboxylate groups of AASs undergoes dissociation; the remaining second sodium ion coordinates both carboxylate groups to form six-, seven-, and eight-membered cyclic conjugated rings in $C_{12}\text{MalNa}_2$, $C_{12}\text{AspNa}_2$, and $C_{12}\text{GluNa}_2$, respectively, as discussed previously. With increasing α_{AAS} , the size of the mixed micelles gradually decreases as summarized in Table 2. In the case of the AASs + HTAB surfactant mixture,

Table 2. d_h , PDI, and η^0 Values at Different α_{AAS} Values in AASs-HTAB Mixed Surfactant Systems at 298 K

α_{AAS}	d_h/nm	PDI	η^0/cP
HTAB-malonate			
1.0	2.20	0.46	1.38
0.8	27.0	0.64	2.30
0.6	30.0	0.38	4.60
0.5	41.5	0.41	23.3
0.4	76.4	0.29	60.2
0.2	86.5	0.45	71.5
0.0	1.30	0.27	18.5
HTAB-aspartate			
1.0	2.80	0.46	1.71
0.8	17.0	0.61	1.29
0.6	21.2	0.54	3.40
0.5	56.4	0.39	19.0
0.4	65.8	0.30	58.6
0.2	78.2	0.46	64.4
HTAB-glutamate			
1.0	3.60	0.38	5.70
0.8	12.0	0.38	0.60
0.6	17.7	0.45	2.37
0.5	23.8	0.28	15.3
0.4	60.2	0.47	55.5
0.2	68.6	0.48	60.0

the maximum number of HTAB molecules accumulates in the micelle, which indicates that HTAB plays a fundamental role in exhibiting higher aggregation and an enhancement of the size and it follows the sequence $C_{12}\text{MalNa}_2 + \text{HTAB} > C_{12}\text{AspNa}_2 + \text{HTAB} > C_{12}\text{GluNa}_2 + \text{HTAB}$. In the case of mixed micelles, the formation of less compact yet rigid aggregates results in a size enhancement, and the results can be correlated with the micellar aggregation number and the area minimum (A_{min}) in

the micelle. Viscosity studies further support the proposition, as will be discussed in the subsequent section.

The PDI value of HTAB is greater than 0.4, and the photon count rate is relatively low. However, for all other systems, the PDI values are less than 0.6 and the count rates are very high. The results are shown in Table 2. Two major peaks are recorded at 3 and 25–30 nm for the mixed surfactant systems, which indicate the formation of small micelles along with other types of larger aggregates.

Viscosity Studies. AASs assorted with HTAB at different ratio are mainly viscous in nature. Viscosity at fixed shear rate (η) vs α_{AAS} profiles is shown Figure 4B. Viscosity decreases with shear rate, indicating the thixotropic behavior of the aggregates. AAS + HTAB mixed surfactants with 20 to 40 mol % AASs are highly viscous (gelatinous) and pass through maxima with increasing α_{AAS} according to the sequence $\text{C}_{12}\text{MalNa}_2 + \text{HTAB} > \text{C}_{12}\text{AspNa}_2 + \text{HTAB} > \text{C}_{12}\text{GluNa}_2 + \text{HTAB}$. Carboxylate groups of AASs are separated by methylene groups, thus while moving from $\text{C}_{12}\text{MalNa}_2$ to $\text{C}_{12}\text{AspNa}_2$ to $\text{C}_{12}\text{GluNa}_2$, the distance between two polar headgroups increases by one carbon atom sequentially. In consonance with the increasing hydrophobic force of interaction between the two oppositely charged headgroups, we have the sequence $\text{C}_{12}\text{MalNa}_2\text{-HTAB} > \text{C}_{12}\text{AspNa}_2\text{-HTAB} > \text{C}_{12}\text{GluNa}_2\text{-HTAB}$. It is proposed that during rotation, surfactant molecules are oriented in the perpendicular direction to form a vertical angle with respect to the rheological plate and accomplish entanglement efficiency. Initially, the viscosity sharply increases up to a particular point with increasing shear rate until 97 s^{-1} , which then gradually decreases due to the shear thinning where entanglement effects are overpowered by the rotational drag, even to zero.⁵⁷ In the case of $\text{C}_{12}\text{GluNa}_2\text{-HTAB}$ mixtures, for 40 mol % $\text{C}_{12}\text{GluNa}_2$, viscosity increases with increasing temperature. Such an unusual phenomenon is due to the formation of wormlike micelles, leading to the viscoelasticity probably contributed by the larger and more complex aggregates in this temperature range. The $\text{C}_{12}\text{GluNa}_2\text{-HTAB}$ mixture is fashioned (a bit) into disordered aggregates, and the aggregate ordering stops at a certain stage as a result of the kinetic reason. This is because the solution has already achieved fluidity through the rearrangement of the chains; however, this is an even more ordered layer and hence is even more viscous. The second maximum with 40 mol % AAS in viscosity vs α_{AAS} is even higher, probably contributed by the higher aggregation number of HTAB as the polar headgroup of HTAB closely interacts in the micelle. The results are well correlated with the DLS studies. η^0 vs α_{AAS} profiles for the three different surfactant mixtures are shown in Figure 5. With increasing α_{AAS} , η^0 decreases where the decrease profile obey the two-degree polynomial fit with regression coefficient values close to 0.99. The results are shown in Table 2.

In the case of the AAS + HTAB mixed systems, particularly with 20–40 mol % AAS, higher η^0 values indicate the formation of larger aggregates because they are mainly highly viscous and even in the gel states. Initially, a 3-fold increase in the η^0 value is noted. The aggregation numbers of $\text{C}_{12}\text{MalNa}_2$, $\text{C}_{12}\text{AspNa}_2$, and $\text{C}_{12}\text{GluNa}_2$ are 37, 51, and 49, respectively. This is due to the presence of a smaller number of AASs molecules in the micelle where more fluidlike entities are probable.⁵⁷ Thus, it can be concluded that strong electrostatic interaction among the oppositely charged surfactants results in the formation of viscous or gel-like materials. However, further

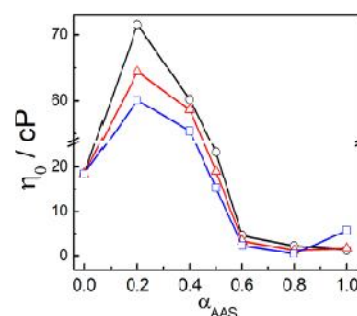


Figure 5. Variation of η^0 with α_{AAS} . Systems: \circ , $\text{C}_{12}\text{MalNa}_2\text{-HTAB}$; Δ , $\text{C}_{12}\text{AspNa}_2\text{-HTAB}$; and \square , $\text{C}_{12}\text{GluNa}_2\text{-HTAB}$. Surfactant solutions (150 mM) at 298 K were used.

structural investigations on the formation of liquid crystals or a gel network, through phase contrast microscopy, polarization optical microscopy (POM), fluorescence microscopy (FM), electron microscopy (SEM), and small-angle X-ray scattering (SAXS) studies, are warranted. These are considered to be future perspectives.

CONCLUSIONS

The aforementioned set of studies focused on comprehensive analyses of the micellization behavior of oppositely charged mixed surfactant systems with the amino acid-based dicarboxylic acid surfactants and HTAB, which were not systematically reported earlier. Such comprehensive studies could shed further light on the oppositely charged mixed surfactant systems. Besides, the generated data on mixed micelles are also considered to be important for further theoretical investigation, where the different micellar parameters can be derived using different theoretical propositions.^{7,19,58,59} Interfacial behavior and micellization behavior of AASs-HTAB mixtures were studied using different physicochemical techniques. Substantially lower CMC value of the surfactant mixtures compared to the predicted values reveal an associative interaction between the oppositely charged surfactants.^{6–9,19} A negative Gibbs free energy of micellization indicates the spontaneity of the micellization process.^{5,60} With increasing α_{AAS} , the surface pressure at the CMC (π_{CMC}) passes through minima because of the associative interaction between the oppositely charged surfactant mixtures.^{6–9,19} Oppositely charged surfactants can achieve proximities to each other through electrostatic interaction and interact mainly at the micellar surface.⁵ Limiting molecular areas of the mixed surfactant systems at the air–liquid interface gradually decrease, and the surface excess values increase with decreasing α_{AAS} , which is due to the higher hydrophilicity of the AASs. Conductance studies show that a maximum number of surfactant molecules are in their dissociated forms near the CMC, so the micellar surface charge density is higher.⁵² Micellar size gradually increases with decreasing α_{AAS} as a result of the presence of a higher proportion of HTAB in the micelle. Rheological studies provide additional information on the internal structure of mixed surfactant aggregates. During micellization, a maximum number of HTAB molecules occupy the micelles, leading to the formation of close-packed aggregated structures. Oppositely charged surfactants in their mixed states can form different viscous and gelatinous entities.⁵⁷ Viscosity studies reveal the thixotropic nature of the mixed surfactant systems

where viscosity did not change spontaneously with increasing α_{MAS} , with few exceptions. Surfactant mixtures form different types of aggregates, so knowledge of the surface morphology by phase contrast, polarization optical microscopic and electron microscopic studies is considered to be essential, as will be carried out in the future. Studies on the interfacial and micellization behavior of mixed surfactants are expected to provide new insights and can be used for electrostatic molecular sequestration and separation,⁴⁴ as drug delivery systems,^{41,61} in dermatological formulations, and in the synthesis of otherwise water-insoluble inorganic nanoparticles.⁶²

■ ASSOCIATED CONTENT

Supporting Information

The Supporting Information is available free of charge on the ACS Publications website at DOI: 10.1021/acs.langmuir.9b02895.

Details on the absorption and emission spectra of pyrene in the presence of varying concentration of surfactant, variation of the CMC of mixed surfactant systems with composition, and spectra/plots for the determination of aggregation numbers of surfactant micelles by the fluorescence quenching method (PDF)

■ AUTHOR INFORMATION

Corresponding Authors

*E-mail: bordes@chalmers.se.

*E-mail: anuttan.patra@LTU.SE.

*E-mail: akpanda@mail.vidyasagar.ac.in. Phone: +913222298379. Fax: +91322275329/297. Cell: +91 9433347210.

ORCID

Romain Bordes: 0000-0002-0785-2017

Amiya Kumar Panda: 0000-0001-8052-2834

Notes

The authors declare no competing financial interest.

■ ACKNOWLEDGMENTS


This work was financially supported by the University Grants Commission (UGC), New Delhi, India, through the UGC-BSR scheme (F.25-1/2014-15(BSR)/7-234/2009(BSR)), UGC-SAP (no. F. 5-9/2015/DRS-II (SAP-II)), and the Department of Science and Technology, government of India, New Delhi, India, through DST-FIST grants [SR/FST/CS-I/2017/7 (C) and no. SR/FST/CS-II-235/2011 (G)]. A.P. gratefully acknowledges financial support from the Centre for Advanced Mining & Metallurgy (CAMM²), Luleå University of Technology.

■ REFERENCES

- (1) Holland, P. M.; Rubingh, D. N. *Mixed Surfactant Systems*; American Chemical Society: Washington, D.C., 1992; Vol. 501, pp 2–30.
- (2) Kronberg, B. Surfactant mixtures. *Curr. Opin. Colloid Interface Sci.* 1997, 2, 456–463.
- (3) Ohshima, H. *Cationic Surfactants: Novel Surrogates of Phospholipids*; John Wiley and Sons: Hoboken, NJ, 2016; Vol. 1, pp 1020–1043.
- (4) Sugihara, G.; Nagadome, S.; Oh, S. W.; Ko, J. S. A review of recent studies on aqueous binary mixed surfactant systems. *J. Oleo Sci.* 2008, 57, 61–92.
- (5) Chen, L. G.; Bermudez, H. Charge Screening between Anionic and Cationic Surfactants in Ionic Liquids. *Langmuir* 2013, 29, 2805–2808.
- (6) Kumar, D.; Azum, N.; Rub, M. A.; Asiri, A. M. Aggregation behavior of sodium salt of ibuprofen with conventional and gemini surfactant. *J. Mol. Liq.* 2018, 262, 86–96.
- (7) Kumar, D.; Hidayathulla, S.; Rub, M. A. Association behavior of a mixed system of the antidepressant drug imipramine hydrochloride and dioctyl sulfosuccinate sodium salt: Effect of temperature and salt. *J. Mol. Liq.* 2018, 271, 254–264.
- (8) Kumar, D.; Rub, M. A.; Azum, N.; Asiri, A. M. Mixed micellization study of ibuprofen (sodium salt) and cationic surfactant (conventional as well as gemini). *J. Phys. Org. Chem.* 2018, 31, No. e3730.
- (9) Mahbub, S.; Rub, M. A.; Hoque, M. A.; Khan, M. A.; Kumar, D. Micellization behavior of cationic and anionic surfactant mixtures at different temperatures: Effect of sodium carbonate and sodium phosphate salts. *J. Phys. Org. Chem.* 2019, 32, e3967.
- (10) von Wandruszka, R. In *Mixed Surfactant Systems*, 2nd ed.; Masahiko, A., Scamehorn, J. E., Eds.; Surfactant Science Series; Marcel Dekker: New York, 2005; Vol. 127, pp 9657–9658.
- (11) Marques, E.; Khan, A.; da Graca Miguel, M.; Lindman, B. Self-assembly in mixtures of a cationic and an anionic surfactant: the sodium dodecyl sulfate-didodecylmethylammonium bromide-water system. *J. Phys. Chem.* 1993, 97, 4729–4736.
- (12) Ii, H. H.; Imai, Y.; Yamanaka, M.; Hayami, Y.; Takine, T.; Matsubara, H.; Aratono, M. Specific counterion effect on the adsorbed film of cationic surfactant mixtures at the air/water interface. *J. Colloid Interface Sci.* 2011, 359, 189–193.
- (13) Ray, C. B.; Chakraborty, I.; Ghosh, S.; Moulik, S.; Palepu, R. Self-aggregation of alkyltrimethylammonium bromides (C₁₀, C₁₂, C₁₄, and C₁₆TAB) and their binary mixtures in aqueous medium: a critical and comprehensive assessment of interfacial behavior and bulk properties with reference to two types of micelle formation. *Langmuir* 2005, 21, 10958–10967.
- (14) Panda, A. K.; Sarkar, G.; Manna, K. Physicochemical Studies on Surfactant Aggregation. I. Effect of Polyethylene Glycols on the Micellization of SDS. *J. Dispersion Sci. Technol.* 2009, 30, 1152–1160.
- (15) Li, F.; Li, G.-Z.; Chen, J.-B. Synergism in mixed zwitterionic-anionic surfactant solutions and the aggregation numbers of the mixed micelles. *Colloids Surf, A* 1998, 145, 167–174.
- (16) Takehara, H. M. M.; Arakawa, A.; Yoshimura, I.; Yoshida, R. Mixed Micellization of Anionic–Nonionic Surfactants in Aqueous Media: A Physicochemical Study with Theoretical Consideration. *J. Am. Oil Chem. Soc.* 1973, 227.
- (17) Kondo, Y.; Uchiyama, H.; Yoshino, N.; Nishiyama, K.; Abe, M. Spontaneous Vesicle Formation from Aqueous Solutions of Didodecylmethylammonium Bromide and Sodium Dodecyl sulfate Mixtures. *Langmuir* 1995, 11, 2380–2384.
- (18) Maiti, K.; Mitra, D.; Mitra, R. N.; Panda, A. K.; Das, P. K.; Rakshit, A. K.; Moulik, S. P. Self-aggregation of synthesized novel bolaforms and their mixtures with sodium dodecyl sulfate (SDS) and cetyltrimethylammonium bromide (CTAB) in aqueous medium. *J. Phys. Chem. B* 2010, 114, 7499–7508.
- (19) Manna, K.; Chang, C.-H.; Panda, A. K. Physicochemical studies on the cationics of alkyltrimethylammonium bromides and bile salts in aqueous media. *Colloids Surf, A* 2012, 415, 10–21.
- (20) Ogino, K.; Abe, M. *Mixed Surfactant Systems*; CRC Press, 1992.
- (21) Shiloach, A.; Blankshtein, D. Prediction of Critical Micelle Concentrations and Synergism of Binary Surfactant Mixtures Containing Zwitterionic Surfactants. *Langmuir* 1997, 13, 3968–3981.
- (22) Rosen, M. J.; Dahanayake, M. *Industrial Utilization of Surfactants: Principles and Practice*; AOCS Press: Champaign, IL, 2000; pp 28–29.
- (23) Rosen, M. J.; Kunjappu, J. T. *Surfactants and Interfacial Phenomena*, 4th ed.; Wiley: New York, 2012; p 616.
- (24) Kaler, E.; Murthy, A.; Rodriguez, B.; Zasadzinski, J. Spontaneous vesicle formation in aqueous mixtures of single-tailed surfactants. *Science* 1989, 245, 1371–1374.

- (25) Khan, A.; Marques, E. Catanionic surfactants. In *Specialist Surfactants*; Robb, I. D., Ed.; Springer: Dordrecht, The Netherlands, 1997; pp 37–80.
- (26) Kuo, A.-T.; Chang, C.-H. Cholesterol-Induced Condensing and Disordering Effects on a Rigid Catanionic Bilayer: A Molecular Dynamics Study. *Langmuir* 2014, 30, 55–62.
- (27) Kuo, J.-H. S.; Jan, M.-S.; Chang, C.-H.; Chiu, H.-W.; Li, C.-T. Cytotoxicity characterization of catanionic vesicles in RAW 264.7 murine macrophage-like cells. *Colloids Surf., B* 2005, 41, 189–196.
- (28) Yu, W.-Y.; Yang, Y.-M.; Chang, C.-H. Cosolvent Effects on the Spontaneous Formation of Vesicles from 1:1 Anionic and Cationic Surfactant Mixtures. *Langmuir* 2005, 21, 6185–6193.
- (29) Hao, J.; Hofmann, H. Self-assembled structures in excess and salt-free catanionic surfactant solutions. *Curr. Opin. Colloid Interface Sci.* 2004, 9, 279–293.
- (30) Horbaschek, K.; Hoffmann, H.; Hao, J. Classic L_2 Phases as Opposed to Vesicle Phases in Cationic-Anionic Surfactant Mixtures. *J. Phys. Chem. B* 2000, 104, 2781–2784.
- (31) Jiang, Y.; Li, F.; Luan, Y.; Cao, W.; Ji, X.; Zhao, L.; Zhang, L.; Li, Z. Formation of drug/surfactant catanionic vesicles and their application in sustained drug release. *Int. J. Pharm.* 2012, 436, 806–814.
- (32) Marques, E. F. Size and Stability of Catanionic Vesicles: Effects of Formation Path, Sonication, and Aging. *Langmuir* 2000, 16, 4798–4807.
- (33) Beheshteh, S.; Hussein, G.; Behnoosh, T.; Soheila, J.; Majid, H. Molecular Interactions of Cationic and Anionic Surfactants in Mixed Monolayers and Aggregates. *J. Phys. Chem. B* 2008, 112, 14869–14876.
- (34) Herrington, K. L.; Kaler, E. W.; Miller, D. D.; Zasadzinski, J. A.; Chirivolu, S. Phase behavior of aqueous mixtures of dodecyltrimethylammonium bromide (DTAB) and sodium dodecyl sulfate (SDS). *J. Phys. Chem.* 1993, 97, 13792–13802.
- (35) Barker, C. A.; Saul, D.; Tiddy, G. J. T.; Wheeler, B. A.; Willis, E. Phase structure, nuclear magnetic resonance and rheological properties of viscoelastic sodium dodecyl sulphate and trimethylammonium bromide mixtures. *J. Chem. Soc., Faraday Trans. 1* 1974, 70, 154–162.
- (36) Jokela, P.; Jönsson, B.; Wennerström, H. *Phase Equilibria in Systems Containing Both an Anionic and a Cationic Amphiphile: A Thermodynamic Model Calculation*; Steinkopff: Darmstadt, 1985; pp 17–22.
- (37) Hassan, P. A.; Hodgdon, T. K.; Sagasaki, M.; Fritz-Popovskii, G.; Kaler, E. W. Phase behavior and microstructure evolution in aqueous mixtures of cetyltrimethylammonium bromide and sodium dodecyl tri-oxethylene sulfate. *C. R. Chim.* 2009, 12, 18–29.
- (38) Bakshi; Singh, M. Cetylpyridinium chloride + tetradecyltrimethylammonium bromide mixed micelles in polyethylene glycol 1000 + water mixtures. *J. Macromol. Sci., Part A: Pure Appl. Chem.* 1999, 36, 879–892.
- (39) Naidu, P. S. R.; Norret, M.; Smith, N. M.; Dunlop, S. A.; Taylor, N. L.; Fitzgerald, M.; Iyer, K. S. The Protein Corona of PEGylated PGMA-Based Nanoparticles is Preferentially Enriched with Specific Serum Proteins of Varied Biological Function. *Langmuir* 2017, 33, 12926–12933.
- (40) Yingju, F.; Zhipeng, L.; Le, W.; Jinhua, Z. Catanionic-surfactant-controlled morphosynthesis and gas-sensing properties of corundum-type In_2O_3 . *Nanotechnology* 2009, 20, 285501.
- (41) Boudier, A.; Castagnos, P.; Soussan, E.; Beaune, G.; Belkhef, H.; Ménager, C.; Cabuil, V.; Haddioui, L.; Roques, C.; Rico-Lattes, L.; Blanzat, M. Polyvalent catanionic vesicles: Exploring the drug delivery mechanisms. *Int. J. Pharm.* 2011, 403, 230–236.
- (42) Chen, L.; Patrone, N.; Liang, J. F. Peptide Self-Assembly on Cell Membranes to Induce Cell Lysis. *Biomacromolecules* 2012, 13, 3327–3333.
- (43) Li, X.; Kunieda, H. Catanionic surfactants: microemulsion formation and solubilization. *Curr. Opin. Colloid Interface Sci.* 2003, 8, 327–336.
- (44) Lioi, S. B.; Wang, X.; Islam, M. R.; Danoff, E. J.; English, D. S. Catanionic surfactant vesicles for electrostatic molecular sequestration and separation. *Phys. Chem. Chem. Phys.* 2009, 11, 9315–9325.
- (45) Butt, H.-J. Measuring electrostatic, van der Waals, and hydration forces in electrolyte solutions with an atomic force microscope. *Biophys. J.* 1991, 60, 1438–1444.
- (46) Carpena, P.; Aguiar, J.; Bernola-Galván, P.; Carnero Ruz, C. Problems Associated with the Treatment of Conductivity-Concentration Data in Surfactant Solutions: Simulations and Experiments. *Langmuir* 2002, 18, 6054–6058.
- (47) Mansbach, C. M.; Cohen, R. S.; Leff, P. B. Isolation and properties of the mixed lipid micelles present in intestinal content during fat digestion in man. *J. Clin. Invest.* 1975, 56, 781–791.
- (48) Peng, F. F. Surface Energy and Induction Time of Fine Coals Treated with Various Levels of Dispersed Collector and Their Correlation to Flotation Responses. *Energy Fuels* 1996, 10, 1202–1207.
- (49) Spjuth, L.; Liljenzin, J. O.; Skalberg, M.; Hudson, M. J.; Chan, G. Y. S.; Drew, M. G. B.; Feavouri, M.; Iveson, P. B.; Madić, C. The Protein Corona of PEGylated PGMA-Based Nanoparticles is Preferentially Enriched with Specific Serum Proteins of Varied Biological Function. *Radiochim. Acta* 1996, 78, 39.
- (50) Bordes, R.; Holmberg, K. Physical chemical characteristics of dicarboxylic amino acid-based surfactants. *Colloids Surf., A* 2011, 391, 32–41.
- (51) Bordes, R.; Tropsch, J.; Holmberg, K. Counterion specificity of surfactants based on dicarboxylic amino acids. *J. Colloid Interface Sci.* 2009, 338, 529–536.
- (52) Manna, K.; Panda, A. K. Physicochemical studies on the interfacial and micellization behavior of CTAB in aqueous polyethylene glycol media. *J. Surfactants Deterg.* 2011, 14, 563–576.
- (53) Ray, G. B.; Ghosh, S.; Moulík, S. P. Physicochemical studies on the interfacial and bulk behaviors of sodium N-dodecanoyl sarcosinate (SDDS). *J. Surfactants Deterg.* 2009, 12, 131–143.
- (54) Basu Ray, G.; Chakraborty, I.; Moulík, S. P. Pyrene absorption can be a convenient method for probing critical micellar concentration (CMC) and indexing micellar polarity. *J. Colloid Interface Sci.* 2006, 294, 248–54.
- (55) Maiti, K.; Chakraborty, I.; Bhattacharya, S. C.; Panda, A. K.; Moulík, S. P. Physicochemical Studies of Octadecyltrimethylammonium Bromide: A Critical Assessment of Its Solution Behavior with Reference to Formation of Micelle, and Microemulsion with n-Butanol and n-Heptane. *J. Phys. Chem. B* 2007, 111, 14175–14185.
- (56) Clint, J. H. Micellization of mixed nonionic surface active agents. *J. Chem. Soc., Faraday Trans. 1* 1975, 71, 1327–1334.
- (57) Sastry, N. V.; Singh, D. K. Surfactant and gelation properties of acetylsalicylate based room temperature ionic liquid in aqueous media. *Langmuir* 2016, 32, 10000–10016.
- (58) Motomura, K.; Yamanaka, M.; Aratono, M. Thermodynamic consideration of the mixed micelle of surfactants. *Colloid Polym. Sci.* 1984, 262, 948–955.
- (59) Moulík, S.; Ghosh, S. Surface chemical and micellization behaviours of binary and ternary mixtures of amphiphiles (Triton X-100, Tween-80 and CTAB) in aqueous medium. *J. Mol. Liq.* 1997, 72, 145–161.
- (60) Edlund, H.; Sadaghiani, A.; Khan, A. Phase Behavior and Phase Structure for Catanionic Surfactant Mixtures. Dodecyltrimethylammonium Chloride-Sodium Nonanoate-Water System. *Langmuir* 1997, 13, 4953–4963.
- (61) Svenson, S. *Carrier-Based Drug Delivery*; American Chemical Society: Washington, D.C., 2004; Vol. 879, pp 2–23.
- (62) Leontidis, E.; Kleitou, K.; Kyprianidou-Leodidou, T.; Bekiari, V.; Lianos, P. Gold Colloids from Cationic Surfactant Solutions. I. Mechanisms That Control Particle Morphology. *Langmuir* 2002, 18, 3659–3668.

Theoretical Approaches on the Synergistic Interaction between Double-Headed Anionic Amino Acid-Based Surfactants and Hexadecyltrimethylammonium Bromide

Manas Barai¹ · Manas Kumar Mandal¹ · Habiba Sultana¹ · Emili Manna² · Sourav Das³ · Kaushik Nag⁴ · Soumen Ghosh³ · Anuttam Patra⁵ · Amiya Kumar Panda¹ 

Received: 1 October 2019 / Revised: 11 March 2020 / Accepted: 15 March 2020
© 2020 AOCS

Abstract Theoretical investigations on the micellization of mixtures of (i) amino acid-based anionic surfactants [AAS: *N*-dodecyl derivatives of aminomalonate, –aspartate, and –glutamate] and (ii) hexadecyltrimethylammonium bromide (HTAB), were carried out at different mole ratios. Variation in the theoretical values of critical micelle concentration (CMC), mole fraction of surfactants in the micellar phase (X), at the interface (X^σ), interaction parameters at the bulk/interface (β^R/β^σ), ideality/nonideality of the mixing processes, and activity coefficients (f) were evaluated using Rubingh, Rosen, Motomura, and Sarmoria-Puvvada-Blankschtein models. CMC values significantly deviate from the theoretically calculated values, indicating associative interaction. With increasing mole fraction of AAS (α_{AAS}), the magnitude of the (β^R/β^σ) values gradually decreased, considered to attributable to hydrophobic interactions. With increasing α_{AAS} , the micellar mole fraction of HTAB (X_2) decreased insignificantly and

X_2 values were higher than those compared to AAS for all combinations, due to the dominance of HTAB in micelles. Micellar mole fraction at the ideal state of AAS (X_1^{ideal}) differed from micellar mole fraction of AAS (X_1), indicating nonideality in the mixed micellization process. Gibbs free energy of micellization (ΔG_m) values are more negative than the free energy of micellization for ideal mixing ($\Delta G_m^{\text{ideal}}$), indicating the micellization process is spontaneous. With increasing α_{AAS} , the enthalpy of micellization (ΔH_m) and entropy of micellization (ΔS_m) values gradually increased, which indicates micellization is exothermic. The different physicochemical parameters of the mixed micelles are correlated with the variation in the spacer length between the two carboxylate groups of AAS.

Keywords Mixed micelle · Synergism · Interaction parameter · Micellar composition · Activity coefficient

Supporting information Additional supporting information may be found online in the Supporting Information section at the end of the article.

J Surfact Deterg (2020).

✉ Amiya Kumar Panda
akpanda@mail.vidyasagar.ac.in

- ¹ Department of Chemistry, Vidyasagar University, Midnapore, West Bengal 721102, India
- ² Centre for Life Sciences, Vidyasagar University, Midnapore, West Bengal 721102, India
- ³ Centre for Surface Science, Department of Chemistry, Jadavpur University, Kolkata, West Bengal 700032, India
- ⁴ Department of Biochemistry, Memorial University of Newfoundland, St. John's, Canada
- ⁵ Chemistry of Interfaces Group, Luleå University of Technology-SE-97187, Luleå, Sweden

Abbreviations

α_{AAS}	mole fraction of AAS
α_i	stoichiometric mole fraction
β^R, β^σ	interaction parameters at the bulk and interface
$\Delta H_m, \Delta G_m$ and ΔS_m	changes in enthalpy, free energy and entropy of micellization
$\Delta G_m^{\text{ideal}}$	free energy of micellization for ideal mixing
Γ_{max}	surface excess
A_{min}	minimum molecular area of the surfactant at the air-water interface

π_{CMC}	surface pressure at the <i>CMC</i>
ΔG_{mic}^0	change in the standard free energy of micellization
$\Delta G_{mic}^0, free$ energy of adsorption	Gibbs free energy of interfacial adsorption
$(\Delta G_{ads}^0)\Delta G_{ads}^0$ X^σ, X_1^σ	mole fraction of surfactant and AAS at the micellar interface
β	synergistic interaction
β_{12}	specific interaction between AAS and HTAB
α^*	predicted optimal micellar composition
AAS	amino acid based anionic surfactant
C_1, C_2 and C_{mix}	molar concentrations of AASs, HTAB and mixture
<i>CMC</i>	critical micelle concentration
CMC_{cal}, CMC_{av}	theoretically calculated <i>CMC</i> and average <i>CMC</i>
CMC_i	<i>CMC</i> of i^{th} component
$C_{12}MalNa_2,$ $C_{12}AspNa_2$ and $C_{12}GluNa_2$	disodium salt of <i>N</i> -dodecyl aminomalonate, aspartate, glutamate
f_i, f_1 and f_2	Activity coefficient, activity coefficient of AAS and HTAB
f_i, f_i^0	surface activity and activity coefficient of i^{th} component
G^{Ex}	excess free energy of micellization
H^{Ex}	excess enthalpy
HTAB	Hexadecyltrimethylammonium bromide
n	aggregation number
QB64	Q-basic 64-data base
RST	regular solution theory
SPB	Sarmoria-Puvvada-Blankshchein
X, X_1 and X_2	mole fraction of AAS and HTAB
X_1^{ideal}	micellar mole fraction at the ideal state of AAS
X_{AAS}, X_{HTAB}	micellar composition of AAS and HTAB
X_1^σ	mole fraction of AAS at the interface
X_{SPB}	<i>CMC</i> values calculated by SPB model

Introduction

Synergistic interaction between two oppositely charged surfactants in aqueous medium mainly depends on the

composition, and environmental parameters such as temperature, pressure, salinity, and solvent type are of secondary importance (Holland and Rubingh, 1992; Kronberg, 1997; Ohshima, 2016; Sugihara et al., 2008). They also exhibit significantly lower critical micellar concentration (*CMC*) compared to the surfactants in neat form. Hydrophobic interactions and nonsystematic interfacial packing also result in lower *CMC* (Vonwandruszka, 2005). Studies of mixed surfactants include cationic/anionic, (Marques et al., 1993) cationic/cationic, (Li et al., 2011) cationic/non-ionic, (Ray et al., 2005) anionic/non-ionic (Panda et al., 2009), and zwitterionic/anionic (Li et al., 1998) systems, among others. Many mixed surfactant systems exhibit synergistic interactions, resulting in a *CMC* that is considerably lower than the *CMC* of the constituent surfactants, suitable for applications (Scamehorn, 1986).

The present work describes a theoretical investigation on the mixing behavior, synergistic interaction, and structural parameters in the molecular level for the mixed micelles of three synthesized dicarboxylic amino acid-based surfactants (AAS: *N*-dodecyl derivatives of amino-malonate, -aspartate and -glutamate in combination with hexadecyltrimethylammonium bromide (HTAB). We have investigated the interfacial and micellar aggregation behavior using different experimental techniques, such as, conductivity, surface tension, ultraviolet-visible (UV-vis) absorption/emission spectroscopy, and dynamic light scattering, to determine different physicochemical parameters, viz., surface excess (Γ_{max}), minimum molecular area at the air-water interface (A_{min}), surface pressure at the *CMC* (π_{CMC}), change in the standard free energy of micellization (ΔG_{mic}^0), $\Delta G_{mic}^0, free$ energy of adsorption (ΔG_{ads}^0) Gibbs free energy of interfacial adsorption (ΔG_{ads}^0), and aggregation number (n) (Barai et al., 2019; Manna et al., 2012). As a continuation of the earlier works, well established theoretical formalisms were used to describe the micellization behavior of structurally heterogeneous surfactant mixtures (Mahbub et al., 2019). However, the formalisms are not predictive; as the experimentally fitted empirical interaction parameter values are mixture dependent. Previously determined experimental *CMC* values for the pure as well as mixed systems of AAS and HTAB were used and subsequently analyzed using different computerized models to evaluate the composition and interaction parameters among the components at the air-water interface and as well as in the micellar phase. Clint's phase separation model relates the mole fraction and *CMC* of mixed components in the case of ideal mixing (Clint, 1975). Rubingh et al. (Coret et al., 1999) established a theoretical model on the basis of regular solution theory (RST); this theory predicts the interaction between the constituent surfactants. Gu and Rosen (1989) extended the Rubingh model from bulk phase behavior to the monolayer at the air-water interface. Motomura et al. (1984) proposed

the mixed micellar model based on ideal consideration, which implies that there occurs no interaction (either attractive or repulsive, between the surfactant components). Sarmoria et al. (1992) have proposed mixed micelle formation involving a surfactant-based phase separation model. Puvvada and Blankschtein (1992) developed a molecular thermodynamics theory in developing the binary and ternary mixed surfactant systems. In the present work, all the aforementioned formalisms were taken into account in analyzing the different structural and compositional parameters of mixed micelles of different combinations (Chakraborty and Ghosh, 2008).

In order to shed further light in this field of research, the present work endeavors to study the synergistic interaction between the oppositely charged mixed surfactant systems (Bakshi and Singh, 1999; Hassan et al., 2009). HTAB-AAS mixed systems are highly relevant in terms of their wide range of applications in industries, *viz.*, enhanced oil recovery, (Brackman and Engberts, 1993) wastewater treatment (Goddard, 1994), textile wetting (Lioi et al., 2009), detergency (Bera et al., 2013), paper manufacturing, (Helbig et al., 1998) pharmaceutical production (Upadhyaya et al., 2007), fabrication of nanostructured materials (Yingju et al., 2009), drug delivery (Boudier et al., 2011), cell lysis (Chen et al., 2012), microemulsion formulation (Li and Kunieda, 2003), molecular separation (Brackman and Engberts, 1993), lubrication (Butt, 1991), cleaning operations (Carpena et al., 2002), and antimicrobial activity (Wilkinson et al., 2003). AAS, capable of forming vesicles, shows manifold applications in biochemical research (Hao and Hoffmann, 2004), foaming control, surfactant-based separation (Mansbach et al., 1975), surface wetting modification, and flotation (Peng, 1996). The two carboxylate groups of AAS do not interact prominently with HTAB, because during hydration, polar head groups of AAS associate with water molecules. Hence, AAS alone are not suitable as individual surfactants for the formation of micelles. Because *CMC* values of AAS are relatively high, it is quite rational to combine AAS with HTAB, to achieve a lower *CMC*.

The main aim of this work is to investigate on the structure and composition of mixed micelles in the molecular level using different proposed models, *viz.*, Clint, Rubingh, Rosen, Motomura, and Sarmoria-Puvvada-Blankschtein (SPB). Method of iteration was adopted toward these endeavors. Different thermodynamic parameters of all the three combinations were evaluated from the theoretically calculated and experimentally determined *CMC* values using computation. It is believed that studies on the micellar structure and composition of surfactant mixtures can provide new insights, which will eventually help in understanding its bulk and interfacial properties that would also minimize the experimental circumscription.

Experimental Section

Materials

HTAB was purchased from Sigma-Aldrich Chemicals Pvt. Ltd (St. Louis, MO, USA). Lauroyl chloride, L-aspartic acid, and L-glutamic acid were the products from Acros Organics Pvt. Ltd (Mumbai, India). Aminomalonic acid diethyl ester hydrochloride was purchased from TCI Pvt. Ltd (Tokyo, Japan). Hydrochloric acid, pyridine, and sodium hydroxide were purchased from VWR (Stockholm, Sweden).

Synthesis of the AASs (Amino Acid Based Surfactants)

Synthesis of AAS was described in literature (Bordes et al., 2009; Bordes and Holmberg, 2011).

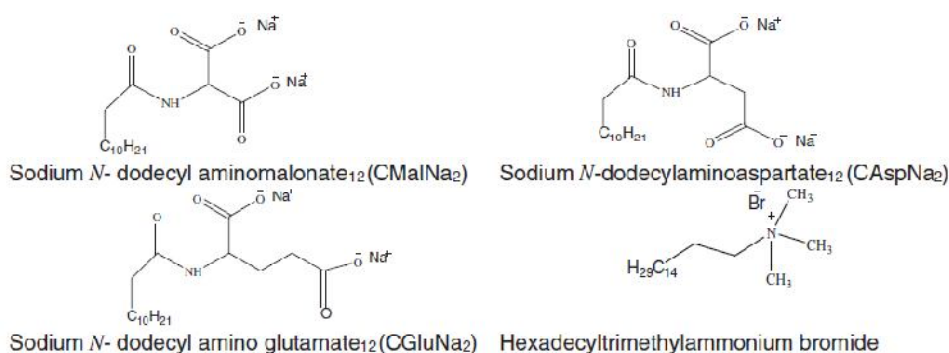
Synthesis of Sodium *N*-Dodecyl Amino Aspartate and Glutamate

A suspension of amino acid (310 mmol) was prepared in a mixture of water/acetone (210 mL/150 mL) mixture in a round-bottom flask. pH was controlled at 12 with an automatic titrator filled with a solution of sodium hydroxide at 2.5 M. Lauroyl chloride was added dropwise under constant stirring at 5 °C and stirring was continued for 90 min. The mixture was then cooled to 0 °C and pH was set at 12 and stirred for 2 h. The solution was warmed at 22 °C and acidified at pH = 2. The white precipitate was then filtered and washed with water. The product was crystallized three times from the toluene. The product was dissolved in ethanol and a solution of sodium hydroxide (2 M) was added, leading to precipitate which was isolated by filtration. The final yields of C₁₂AspNa₂ and C₁₂GluNa₂ were 74% and 76%, respectively.

Synthesis of Sodium *N*-Dodecyl Aminomalonate

The diethyl ester of the amino acid (47 mmol) was dissolved in pyridine (100 mL) in a round-bottom flask. Lauroyl chloride (47 mmol) in THF (100 mL) was added under stirring at room temperature. The suspension was stirred for 18 h and was then poured in 1.5 L (1 M) hydrochloric acid. After 2 h, stirring the solid diethyl ester of dicarboxylate surfactant was filtered, washed with water, and dissolved in ethanol (150 mL). Sodium hydroxide (2 M, 2 eqv.) in ethanol (30 mL) was then added, leading to a white precipitate, which was isolated by filtration. The final purity of C₁₂MalNa₂ was 76%. All the surfactants were found to be more than 98% pure after recrystallization.

Structures of HTAB and the newly synthesized AAS surfactants are shown in Scheme 1.



Scheme 1 Chemical structures of the surfactants.

Instrumentation

Surface Tension Studies

Surface tension was recorded by a du Noüy tensiometer with an accuracy of 0.1 mNm^{-1} (Jencon, Kolkata, India). From the break point of the surface tension *versus*. $\log C$ (surfactant concentration) plot, *CMC* was determined (Barai et al., 2019; Manna et al., 2012).

Conductance Studies

Conductance values were recorded by a direct reading conductivity meter, Con 510 (Eutech Instruments, Singapore) with an accuracy of $\pm 0.1 \mu\text{S cm}^{-1}$. From the break point of the conductance *versus*. $[C]$ plots, *CMC* values were determined (Barai et al., 2019; Manna and Panda, 2011).

UV–vis Absorbance and Emission Spectroscopic Studies

UV–vis absorption spectra were obtained by a spectrophotometer (UVD-2950, Labomed Inc., LA, CA, USA). The sum of the absorbance of pyrene (A_T) was plotted against $[C]$. From the midpoint of the sigmoidal plot, the *CMC* value was calculated (Basu Ray et al., 2006). Fluorescence spectroscopic measurements were performed by a spectrofluorometer (Hitachi High Technologies Fluorescence Spectrophotometer Corporation, F-7100, Tokyo, Japan), where *CMC* was also obtained from the sigmoidal curve, in the I_1/I_3 *versus* $[C]$ plot, where I_1 is the first vibronic peak and I_3 is the third vibronic peak of the pyrene. (Barai et al., 2019; Maiti et al., 2007).

Theoretical *CMC* values were calculated using Clint (1975) formalism. Micellar structure and composition of micelle in the molecular level were calculated using different proposed models, *viz.*, Rubingh's, Rosen, Motomora and SPB. Rubingh's formalism has been successfully utilized to describe and correlate the observed nonidealities in

the micellization behavior in the case of the different surfactants mixtures (Holland, 1986). Different interaction parameters, *viz.*, mole fraction of surfactant at the micellar interface (X^{σ}), interaction parameters at the bulk/ interface (β^R/β^{σ}), activity coefficient (f), and ideality/nonideality of the mixing processes of individual component were evaluated. Calculated using Q-basic 64-data base (QB64) software program. Q-basic is a short form of Quick Beginners. Symbolic instruction code is an integrated development environment (IDE) and interpreter for a variety of BASIC programming languages based on QuickBASIC software. The theoretical values of *CMC* were calculated by different physicochemical processes and its comparison with the experimental values are subsequently discussed (Manna et al., 2012). The average experimental *CMC* values are calculated by different physicochemical processes and their comparison with theoretical *CMC* due to the associative interaction between AAS and HTAB being subsequently discussed (Barai et al., 2019; Manna et al., 2012).

Results and Discussion

Critical Micelle Concentration

CMC of pure HTAB was found to be 0.72 mM (Barai et al., 2019; Manna et al., 2012) while those of disodium salt of *N*-dodecyl aminomalonate ($C_{12}\text{MalNa}_2$), *N*-dodecyl aminoaspartate ($C_{12}\text{AspNa}_2$), and *N*-dodecyl aminoglutamate ($C_{12}\text{GluNa}_2$) were 51.2 , 46.3 , and 36.45 mM , respectively (Barai et al., 2019; Bordes et al., 2009; Bordes and Holmberg, 2011). With increasing mole fraction of amino acid-based surfactant (α_{AAS}), *CMC* values gradually increased from the initial lower value of HTAB as shown in Fig. 1, and also summarized in Table S1. Experimental *CMC* values are lower than the theoretically calculated *CMC* of different AAS + HTAB mixtures (Barai et al., 2019). Significant negative deviation from the theoretically calculated values is due

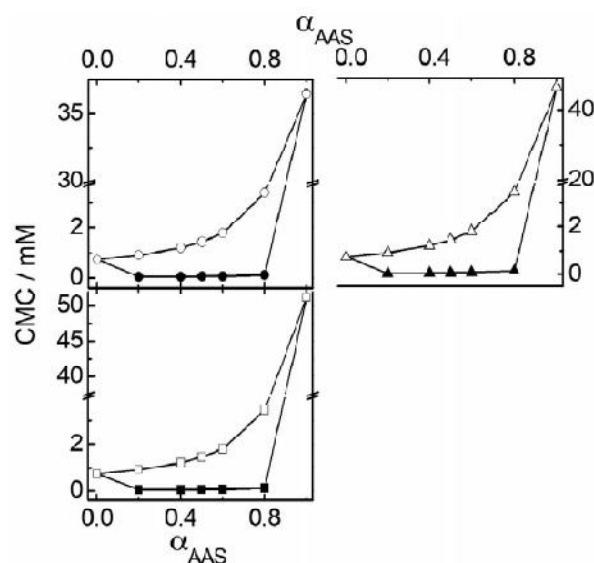


Fig. 1 Variation of CMC with α_{AAS} at 298 K. Systems: \circ , $C_{12}MalNa_2$ -HTAB; Δ , $C_{12}AspNa_2$ -HTAB, and \square , $C_{12}GluNa_2$ -HTAB. Open symbols correspond to the theoretically calculated CMC values using Clint formalism and the closed symbols indicate the experimentally determined average CMC values. Temperature: 298 K

to the associative interaction between the AAS and HTAB (Tikariha et al., 2010). Competitive interfacial adsorption is observed due to the hydrophobic interaction between AAS and HTAB, assisted by charge neutralization in the micelle. Strong attractive interactions between the oppositely charged surfactants in the bulk solvent and interface can be explained using the theoretical models proposed by Clint (Bakshi, 2000; Clint, 1975), (Bakshi et al., 2002; Rosen, 1994), (Arai et al., 1998; Rubingh and Mittal, 1979), and SPB (Sarmoria et al., 1992; Ghosh, 2001). Composition of micelles in the case of oppositely charged mixed surfactants are usually different from the interfacial and bulk compositions (Ghosh, 2001). Synergistic interaction is reflected through the occurrence of substantially lower CMC in the case of surfactant mixtures than the theoretically calculated values. The activity coefficient of surfactant in the micelle (f), interaction parameter between the components of mixed surfactant (β^R), micellar mole fraction of AAS (X_{AAS}), micellar mole fraction of HTAB (X_{HTAB}), mole fraction of AAS at the interface (X_1^σ), and micellar mole fraction of AAS at the ideal state (X_1^{ideal}) values were also evaluated. Components 1 and 2 are the designations of binary components AAS and HTAB, respectively. The Clint model is known to provide reasonable information about the amphiphile mixture in solution. Variation of CMC with the surfactant mole fraction and the micellar composition of binary surfactants can further be assessed using the Clint model as explained in the following section.

Interaction between Oppositely Charged Surfactants and Theoretical Propositions

Clint Model

Surfactants in the bulk solvent and at the air-water interface, exhibit either ideal or nonideal mixing behavior between the components. The CMC value of mixed surfactants can also be theoretically calculated using Clint formalism assuming ideal mixing (Clint, 1975):

$$\frac{1}{CMC_{cal}} = \sum_{i=1}^n \frac{\alpha_i}{CMC_i} \quad (1)$$

where CMC_i is the CMC of neat surfactant “ i ” in solvent and “ n ” is the number of surfactants in the mixture. It is observed that the average experimental CMC values, which correspond to the average of the CMC values determined by surface tension, conductivity, and UV-vis absorption/emission spectroscopy) of mixed surfactants at different mole fractions exhibit significant negative deviations from theoretically calculated CMC (CMC_{cal}), indicating associative interaction among the oppositely charged surfactants, as shown in Fig. 1. A secondary cause of this trend for AAS-HTAB mixtures is the enhanced hydrophobicity through the formation of pseudo-double tailed entities (formed by the cationic and anionic surfactants) and ion pairing of the surfactant head groups (Manna et al., 2012). In the case of *N*-dodecyl amino malonate, there is only one carbon atom in between two carboxylate groups. In the case of aspartate and glutamate, the number of carbon atoms between the two carboxylate moieties are two and three, respectively. The sequential increase in the number of carbon atoms that act as spacer between the two carboxylate moieties favor micellization due to enhanced hydrophobicity. The progressive enhancement in the hydrophobicity, contributed by the methylene group between the two carboxylate groups, also favors negative deviation in the experimental CMC values (Mao et al., 2019). It is expected that the structural difference between HTAB and AAS is the most important causative factor for the deviations of experimental and theoretical CMC . With increasing hydrophobicity of the spacer, synergistic interaction between HTAB and the AAS also increases. Therefore, hydrophobic interactions between the monomers of the surfactant pair at the air-water interface likely follow the extent of deviation between theoretical and measured CMC : $C_{12}MalNa_2 + HTAB > C_{12}AspNa_2 + HTAB > C_{12}GluNa_2 + HTAB$. The Clint model fails to properly explain (i) the deviation of experimental CMC from the CMC_{cal} (using Equation (1)) based on an ideal mixture, (ii) interaction among different surfactants in the aggregated state, (iii) the micellization behavior for concentrated solutions (systems with very high CMC), and (iv) the ability of mixed surfactants in forming the micelles that enhance the hydrophobic

environment in comparison to the micelles formed by neat HTAB or AAS. Rosen et al. (Gu and Rosen, 1989) modified Clint's model with the following propositions: (i) the mole fraction of a particular component in the micelle is lower than the mole fraction of the component in the overall solution, indicating a lower extent of transfer from solution to micelle, (ii) mixtures show synergism, and (iii) increasing hydrophobicity leads to increasing synergistic interaction.

Rosen Model

The Rosen model can assess the interaction between oppositely charged surfactants for the formation of mixed monolayer at the air-water interface (Rosen, 1994). Using RST (Rubingh and Mittal, 1979) and standard surface tension methods (Rosen and Hua, 1982), the composition of individual components in the mixed monolayer, mole fraction of AAS at the interface, (X_1^σ) and interfacial interaction parameter (β^σ) can be evaluated. β^σ at the air-water interface was proposed using the "successive method" (method of iteration, as described below) (Rosen and Dahanayake, 2000; Rosen and Kunjappu, 2012), assuming the formation of monolayer at the air-water interface. For this purpose, a computer program was made to estimate β^σ and micellar mole fraction of AAS in the air-water interface X_1^σ via the following equations (Rosen and Kunjappu, 2012):

$$\frac{(X_1^\sigma)^2 \ln(X_1 C_{av}/X_1^\sigma C_1)}{(1-X_1^\sigma)^2 \ln[1-X_1 C_{av}/(1-X_1^\sigma) C_2]} = 1 \quad (2)$$

$$\beta^\sigma = \frac{\ln(X_1 C_{av}/X_1^\sigma C_1)}{(1-X_1^\sigma)^2} \quad (3)$$

β^σ versus α_{AAS} profiles are shown in Fig. 2 (panel B). With increasing α_{AAS} , the magnitude of β^σ gradually decreases for each AAS. The synergistic interaction (β^σ) between AAS and HTAB at the air-water interface follows the sequence $\text{C}_{12}\text{MalNa}_2 + \text{HTAB} > \text{C}_{12}\text{AspNa}_2 + \text{HTAB} > \text{C}_{12}\text{GluNa}_2 + \text{HTAB}$. Increasing the number of

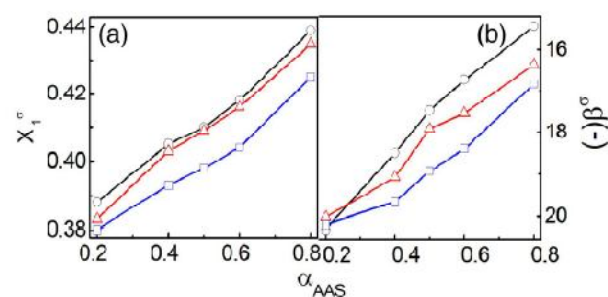


Fig. 2 Variation of X_1^σ and β^σ calculated from Rosen model with the mole fraction of α_{AAS} at 298 K. systems: O, $\text{C}_{12}\text{MalNa}_2\text{-HTAB}$; Δ , $\text{C}_{12}\text{AspNa}_2\text{-HTAB}$, and \square , $\text{C}_{12}\text{GluNa}_2\text{-HTAB}$

methylene groups between the carboxylates sterically favors its interaction with HTAB. The increased electrophilic interaction between the two oppositely charged head groups, inducing formation of mixed micelles, can explain the above sequence of β^σ (Huang and Ren, 2019; Ren, 2015; Ren et al., 2016; Ren et al., 2017a, 2017b; Ren et al., 2018). On the other hand, the close proximity of the two carboxylate groups of AAS enhances electrostatic repulsion. X_1^σ versus α_{AAS} profiles are shown in Fig. 2 (panel A). Unlike β^σ , X_1^σ gradually increases with increasing α_{AAS} , which suggest that HTAB interacts less favorably with AAS at the air-water interface to form mixed monolayer. With increasing α_{AAS} , X_2 and $(1 - X_1^\sigma)$ values gradually decreased, which indicates that the mixed micelles contain a larger proportion of HTAB compared to the overall solution, as a result of a smaller cross sectional area and higher hydrophobicity for HTAB (Manna et al., 2012). For all compositions, X_2^σ follows the order: $\text{C}_{12}\text{MalNa}_2 < \text{C}_{12}\text{AspNa}_2 < \text{C}_{12}\text{GluNa}_2$. The same trend is also reflected by lower aggregation number of $\text{C}_{12}\text{MalNa}_2$ compared to $\text{C}_{12}\text{AspNa}_2$ and $\text{C}_{12}\text{GluNa}_2$, (Fig. S1) (Barai et al., 2019). The trend can be explained by $\text{C}_{12}\text{MalNa}_2$ being less bulky and hydrophilic than the other two AAS due to the absence of methylene group between two carboxylate anions, thereby enabling $\text{C}_{12}\text{MalNa}_2$ to more strongly interact with HTAB and remain associated with the micellar surface (Pal and Saini, 2019). The stronger interaction between $\text{C}_{12}\text{MalNa}_2$ and HTAB are also reflected by lower β^σ values (Table S1) (Huang and Ren, 2019; Ren, 2015; Ren et al., 2016; Ren et al., 2017a, 2017b; Ren et al., 2018). Negative β^σ values for all the AAS+HTAB mixed micelles also indicate mutual interaction between the monomers of surfactant pair at the air-water interface (Bakshi et al., 2002). The values of X_1^σ for all the three binary surfactant mixtures are smaller than $X_1(\alpha_{\text{AAS}})$, indicating that AAS are less prominent at the air-liquid interface than HTAB.

Rubingh Model

Clint's proposition about the stronger deviation of experimental CMC with respect to theoretical CMC was also addressed by Rubingh. Rubingh's model for ideal/nonideal mixed systems is based on RST. Thus, following modification of the Equation (1) was made according to the proposition of Rubingh (Rubingh and Mittal, 1979):

$$\frac{1}{\text{CMC}} = \sum_{i=1}^n \frac{\alpha_i}{f_i \text{CMC}_i} \quad (4)$$

where, f_i is the activity coefficient of i^{th} component in a micelle. Molecular interaction parameters were studied in the light of RST (Rubingh and Mittal, 1979). Unlike the models described above, RST is capable to predict the

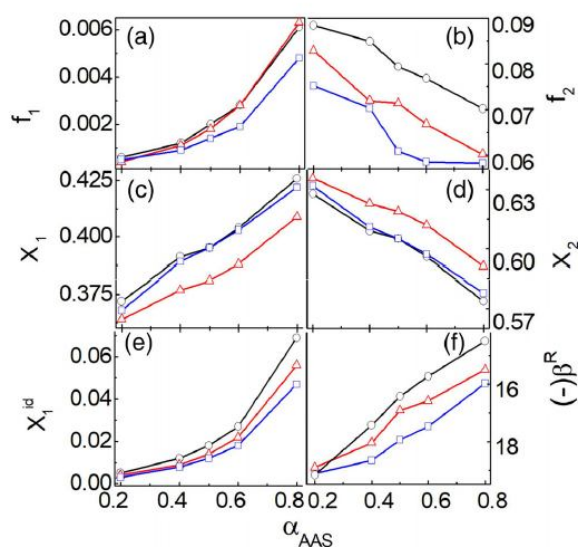


Fig. 3 Variation of f_1 , f_2 , X_{AAS} , and X_{HTAB} values, calculated using Rubingh's model, X_1^{ideal} and β^{R} values, calculated using Motomura equation with the mole fraction of α_{AAS} at 298 K. systems: O, $\text{C}_{12}\text{MalNa}_2\text{-HTAB}$; Δ , $\text{C}_{12}\text{AspNa}_2\text{-HTAB}$, and \square , $\text{C}_{12}\text{GluNa}_2\text{-HTAB}$

synergistic as well as antagonistic interaction between the surfactant mixture. The f_1 and f_2 versus α_{AAS} profiles are shown in Fig. 3 (panels A and B, respectively). With increasing α_{AAS} , f_1 values increase while the f_2 values decrease. Extent of increase in f_1 values are less than the decrease in f_2 values for all the combinations. The decrease of f_2 values follow the order $\text{C}_{12}\text{MalNa}_2 + \text{HTAB} > \text{C}_{12}\text{AspNa}_2 + \text{HTAB} > \text{C}_{12}\text{GluNa}_2 + \text{HTAB}$. CMC values for the mixtures are similar to the CMC of pure HTAB, indicating that HTAB plays fundamental role for the synergism. Higher values of f_2 (HTAB) than f_1 (AAS) indicate the significant contribution of HTAB due to its larger head group size (Fig. S1). Using RST, Rubingh proposed Equations (4)–(7) for determining different parameters of micellization of binary surfactants (Holland and Rubingh, 1992; Rubingh and Mittal, 1979):

$$\beta^{\text{R}} = \left(\ln \left[\frac{(\text{CMC}_{\text{av}}\alpha_1)}{(\text{CMC}_1(1-X_2)^2)} \right] \right) \quad (5)$$

where, β^{R} is the interaction parameter between the components in the micelle. Micellar mole fraction of AAS (X_{AAS}) and HTAB (X_{HTAB}) versus α_{AAS} profiles are shown in Fig. 3 (panels C and panel D, respectively). Relative proportion of AAS in the micelles gradually increases with increasing α_{AAS} . Nonideality in the mixing behavior was further rationalized by Rubingh using Equation (6) as (Rubingh and Mittal, 1979):

$$\frac{(1-X_2)^2 \ln \left[\frac{\text{CMC}_{\text{av}}\alpha_1}{\text{CMC}_1(1-X_2)^2} \right]}{(X_2)^2 \ln \left[\frac{\text{CMC}_{\text{av}}\alpha_2}{(\text{CMC}_2 X_2)} \right]} = 1 \quad (6)$$

Equation (6) was employed to solve for X_2 iteratively using a computer program. After obtaining X_2 from Equation (6), β^{R} is calculated from Equation (5). Subsequently, f_1 and f_2 are calculated using Equation (7) (Holland and Rubingh, 1992; Rubingh and Mittal, 1979).

$$f_i = \exp[\beta^{\text{R}}(1-X_i^2)] \quad (7)$$

$f = 1$ indicates ideal mixed surfactant systems. The micellar mole fractions obtained from the Rubingh model have been compared with the micellar mole fraction of AAS at the ideal state (X_1^{ideal}), with the help of Motomura's approximation (Motomura et al., 1984):

$$X_1^{\text{ideal}} = \frac{\alpha_1 \text{CMC}_2}{\alpha_1 \text{CMC}_2 + \alpha_2 \text{CMC}_1} \quad (8)$$

X_1^{ideal} versus α_{AAS} profiles are shown in Fig. 3 (panel E). All of the parameters calculated from Equations (5)–(8) are summarized in Table S1. With increasing α_{AAS} , X_1^{ideal} gradually increases for all three AAS. X_1^{ideal} values follow the order $\text{C}_{12}\text{MalNa}_2 > \text{C}_{12}\text{AspNa}_2 > \text{C}_{12}\text{GluNa}_2$. It is observed from Table S1 that micellar composition of HTAB in the ideal state (X_2^{ideal}), calculated by Motomura's approximation show the greater values than those calculated for RST (Kumar et al., 2018). β^{R} values for all three systems investigated are negative, indicating strong attractive interaction between AAS and HTAB (Huang and Ren, 2019; Ren, 2015; Ren et al., 2016; Ren et al., 2017a, 2017b; Ren et al., 2018). With increasing α_{AAS} , the magnitude of β^{R} values gradually decreases (Fig. 3, panel F). X_1^{ideal} for $\text{C}_{12}\text{MalNa}_2$, $\text{C}_{12}\text{AspNa}_2$ and $\text{C}_{12}\text{GluNa}_2$ differ significantly from X_{AAS} values, calculated by RST. Hence, the micellization of the AAS-HTAB systems is nonideal in nature from the view point of Motomura approximation. β^{R} values for AAS-HTAB systems are found to be composition dependent, in contrast with RST, which assumes β^{R} should remain independent of composition. The composition dependency of β^{R} has also been reported in literature for several surfactant mixtures, manifesting the shortcoming of Rubingh's approach for binary surfactant mixtures (Abdul Rub et al., 2017; Rub et al., 2018).

SPB Model

Motomura et al. (1984) proposed the "SPB" model that estimates the phase separation based on molecular thermodynamics theory, where optimal micellar composition was quantified by SPB for binary surfactant mixtures (Sarmoria

et al., 1992). The Clint equation (Clint, 1975) can be rewritten in the following form:

$$\frac{1}{CMC_{cal}} = \frac{\alpha_1}{f_1 CMC_1} + \frac{\alpha_2}{f_2 CMC_2} \quad (9)$$

Activity coefficients (f_i , where $f_i \neq 1$) are calculated by the following equations (Sarmoria et al., 1992):

$$f_1 = \exp \left[\beta_{12} \frac{(1-\alpha^*)^2}{kT} \right] \quad (10)$$

$$f_2 = \exp \left[\beta_{12} \frac{(\alpha^*)^2}{kT} \right] \quad (11)$$

where, β_{12} is the specific interaction between AAS and HTAB (analogous to the β^R) and α^* is the predicted optimal micellar composition, designated by X_{SPB} (the composition at which the free energy of mixed micellization attains its minimum value) (Sarmoria et al., 1992), k is the Boltzmann constant and T is the temperature in absolute scale. Results are summarized in Table S2 and Fig. 4. With increasing α_{AAS} , f_1 gradually increases, (panels A and B). The X_{SPB} values for all the combinations vary almost linearly with α_{AAS} (panel C). β^R versus α_{AAS} profiles are shown in Fig. 4 (panel D). Negative lower β^R values demonstrate stronger synergistic interaction between AAS and HTAB (Abdul Rub et al., 2017; Rub et al., 2018). β_{12} and α^* values were calculated using trial and error method by means of iteration using the following equation (Sarmoria et al., 1992) by minimizing the standard deviation between the equation's left- and right-hand side:

$$\frac{\beta_{12}(1-2\alpha^*)}{kT} + \ln \frac{\alpha^*}{(1-\alpha^*)} = \ln \frac{\alpha_1 CMC_2}{\alpha_2 CMC_1} \quad (12)$$

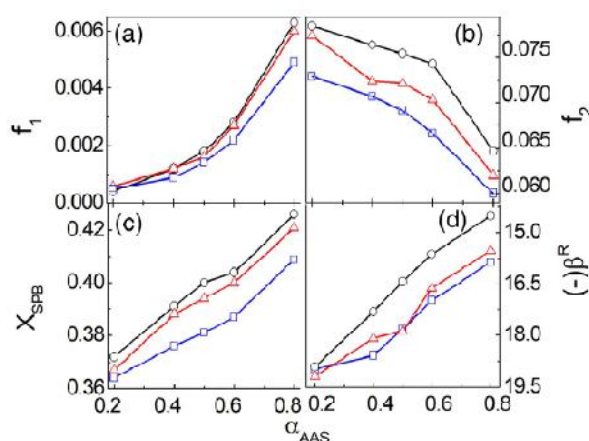


Fig. 4 Variation of f_1 , f_2 and CMC values calculated by SPB model, X_{SPB} and β^R values calculated by SPB model with the mole fraction of α_{AAS} at 298 K. systems: O, $C_{12}MalNa_2$ -HTAB; Δ , $C_{12}AspNa_2$ -HTAB and \square , $C_{12}GluNa_2$ -HTAB

By the substitution of α^* (X_{SPB}) into Equations (11) and (12), β_{12} and f were calculated. From Tables S1 and S2 it is evident that X_{SPB} of various AAS components are comparable with X_{Mal} , X_{Asp} and X_{Glu} calculated using the RST model. Calculated f , β_{12} , and X for the three different systems are nearly the same between Rubingh's and SPB models.

Thermodynamics of Micellization

From the RST model, (Rubingh and Mittal, 1979) different thermodynamic parameters can be derived (Das et al., 2018), assuming that the excess entropy of mixing is zero, as has been performed for other surfactant mixtures (Patel et al., 2017; Ren et al., 2017a, 2017b; Rosen and Kunjappu, 2012; Schulz et al., 2013; Sikorska et al., 2016). Gibbs excess free energy (G^{Ex}), excess enthalpy (H^{Ex}), and enthalpy of micellization (ΔH_m) can be calculated using Equation (13) (Patel et al., 2017; Ren et al., 2017a, 2017b):

$$G^{Ex} = H^{Ex} = \Delta H_m = RT [X_1 \ln (f_1) + X_2 \ln (f_2)] \quad (13)$$

X_1 , X_2 , f_1 , and f_2 values were calculated from Rubingh's model (Rubingh and Mittal, 1979) (Table S1). Gibbs free energy of micellization for ideal mixing ΔG_m^{ideal} can be calculated by the following equation (Patel et al., 2017; Ren et al., 2017a, 2017b):

$$\Delta G_m^{ideal} = RT [X_1 \ln (X_1) + X_2 \ln (X_2)] \quad (14)$$

Gibbs excess free energy ($G^{Ex} = \Delta G_m - \Delta G_m^{ideal}$) indicates the deviation from the ideality for the mixing. ΔG_m designates the nonideal free energy of micellization, given by Equation (15):

$$\Delta G_m = RT [X_1 \ln (X_1 f_1) + X_2 \ln (X_2 f_2)] \quad (15)$$

Changes in entropy of micellization (ΔS_m) can be obtained from Equation (16):

$$\Delta S_m = \frac{\Delta H_m - \Delta G_m}{T} \quad (16)$$

The values of all the parameters discussed above, are presented in Fig. 5 and Table S3. It is evident that with increasing mole fraction of HTAB, ΔH_m increases (Fig. 5, panel A). When comparing the three AAS, it is observed that the ΔH_m values follow the sequence $C_{12}MalNa_2 + HTAB > C_{12}AspNa_2 + HTAB > C_{12}GluNa_2 + HTAB$. There are two opposing factors that contribute to ΔH_m : (i) the energy released due to the loss of translational energy of surfactant monomers as a result of electrostatic and hydrophobic interaction for the micellization, and (ii) energy required to break the organized structure of bulk water. (Schulz et al., 2013;

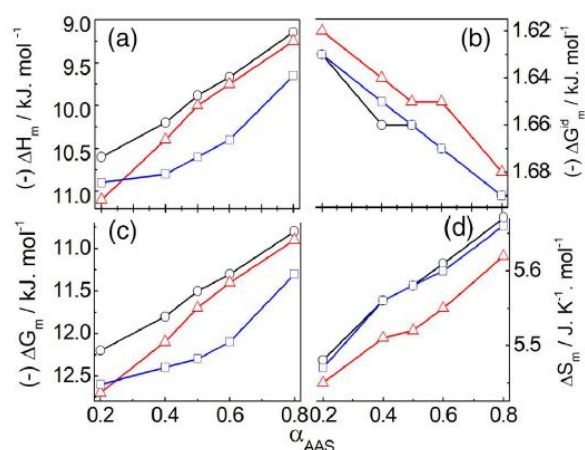


Fig. 5 Variation of G^{Ex} , ΔH_m , H^{Ex} of AAS ($G^{Ex} = \Delta H_m = H^{Ex}$), ΔG_m^{ideal} , ΔG_m , ΔS_m , and β^R values calculated by Rubingh's model with the mole fraction of α_{AAS} at 298 K. systems: O, $C_{12}MalNa_2$ -HTAB; Δ , $C_{12}AspNa_2$ -HTAB and \square , $C_{12}GluNa_2$ -HTAB

Sikorska et al., 2016). As the mole fraction of HTAB is increased, hydrophobic interactions increase, leading to a more exothermic process of micellization. For the same reason, ΔH_m values increase with the sequential increase in the methylene group of the spacer when comparing $C_{12}MalNa_2$ to $C_{12}AspNa_2$ to $C_{12}GluNa_2$. The ΔG_m values are found to be more negative than the ΔG_m^{ideal} , which indicates the spontaneity of micellization (Fig. 5, panel B). The negative values of G^{Ex} further support the occurrence of synergistic interactions (Patel et al., 2017). The same trends are observed for ΔH_m and ΔG_m (Table S3). Variation of ΔG_m for the mixed micelles of HTAB and AASs with α_{AAS} are presented in the panel C of Fig. 5. The entropic contribution of $T\Delta S_m$ toward ΔG_m is found to be 13–16%, which indicates that the entropic contribution (ΔS_m) to the mixed micellization is less than the enthalpic contribution (ΔH_m). With increasing α_{AAS} , ΔS_m values gradually increase, (Fig. 5, panel D), indicating spontaneous micellization and interfacial adsorption. Furthermore, the degree of disorderness increases due to micellization and the entropy change, favorable for the formation of mixed micelles, as demonstrated by the positive ΔS_m values (Patel et al., 2017; Ren et al., 2017a, 2017b).

Conclusions

This theoretical investigation has simplified the molecular thermodynamics-related theory for micelle formation by mixed surfactants systems. Different working models to predict CMC of nonideal binary surfactants as well as

specific interactions were compared. The models provided reasonable quantitative predictions of the different micellization parameters for cationic-anionic mixed surfactant systems. The simplified “working models” employed herein can act as valuable preliminary screening tools in the design and selection of nonideal surfactant mixtures for practical applications. Synergistic interaction behavior of AAS-HTAB mixtures were assessed using Rubingh's, Rosen, Motomura, and SPB models. The experimental CMC values are lower than the predicted values calculated from Clint formalism, indicating nonideality in the mixing behavior. CMC values gradually increase with the increasing proportion of AAS. Oppositely charged surfactants can localize in vicinity to each other and interact mainly at the micellar surface. The two carboxylate groups of AAS repel each other, the extent of which is minimized by HTAB through electrostatic attraction; thus the micellar size gradually decreases with increasing α_{AAS} . A maximum number of HTAB molecules become available on the micellar surface, leading to the formation of closed packed micellar structures (Barai et al., 2019). The binary mixtures show significant synergism (negative β^R value) (Abdul Rub et al., 2017; Rub et al., 2018). With increasing hydrophobicity of the spacer, synergistic interaction between the surfactant components also increase. With increasing α_{AAS} , the magnitude of β^R decreases (Huang and Ren, 2019; Ren, 2015; Ren et al., 2016; Ren et al., 2017a, 2017b; Ren et al., 2018), X_1^{ideal} , X_1 (Rubingh model), and X_1^{σ} (Rosen model) gradually increase with an increase of α_{AAS} . The magnitude of β^{σ} at the air-water interface gradually decreases with increasing α_{AAS} and follows the order $C_{12}MalNa_2 + HTAB > C_{12}AspNa_2 + HTAB > C_{12}GluNa_2 + HTAB$. ΔG_m values are more negative than ΔG_m^{ideal} , which indicate that the micellization process is spontaneous. Mixed micellization of HTAB-AAS is enthalpy driven where ΔH_m values decrease with increasing α_{AAS} (Patel et al., 2017; Ren et al., 2017a, 2017b). It is believed that theoretical investigations of mixed micelles of such binary surfactants can provide new insights, which will eventually help in understanding the bulk and interfacial activities of mixed surfactant systems. Strong synergistic interaction between the oppositely charged surfactants can result in the formation of liquid crystal, viscous gels, and even vesicles. However, further theoretical investigations employing molecular dynamics could support the propositions made here, in the future. Oppositely charged mixed surfactants form different types of aggregates as stated earlier; so the knowledge on the surface morphology by phase contrast, polarization optical microscopy (POM), fluorescence microscopy (FM), field emission scanning electron microscopy (FE-SEM), and small-angle X-ray scattering (SAXS) studies are considered to be essential, being considered to be carried out in future.

ACKNOWLEDGEMENTS This work has been financially supported by University Grants Commission (UGC), New Delhi, India through a UGC-BSR scheme, (F.25-1/2014-15(BSR)/7-234/2009(BSR) UGC-SAP (No. F. 5-9/ 2015/DRS-II (SAP-II) and Department of Science and Technology, Govt. of India, New Delhi, India through the DST-FIST grants (No. SR/FST/CSI-235/2011 (G) and SR/FST/CS-1/2017/7 (C). SD acknowledges CSIR, Govt. of India for senior research fellowship. The authors also convey their deep sense of gratitude to Prof. Douglas Hayes, Editor-in-Chief, Journal of Surfactants and Detergents for his valued guidance in improving the manuscript.

CONFLICT OF INTEREST

The authors declare that they have no conflict of interest.

References

- Abdul Rub, M., Azum, N., & Asiri, A. M. (2017) Binary mixtures of sodium salt of ibuprofen and selected bile salts: Interface, micellar, thermodynamic and spectroscopic study. *Journal of Chemical & Engineering Data*, **62**:3216–3228.
- Arai, T., Takasugi, K., & Esumi, K. (1998) Mixed micellar properties of nonionic saccharide and anionic fluorocarbon surfactants in aqueous solution. *Journal of Colloid and Interface Science*, **197**: 94–100.
- Bakshi, M. S. (2000) Cationic mixed micelles in the presence of β -Cyclodextrin: A host–guest study. *Journal of Colloid and Interface Science*, **227**:78–83.
- Bakshi, M. S., & Singh, M. (1999) Cetylpyridinium chloride + tetradecyltrimethylammonium bromide mixed micelles in polyethylene glycol 1000 + water mixtures. *Journal of Macromolecular Science*, **36**:879–892.
- Bakshi, M., Sachar, S., Mahajan, N., Kaur, I., Kaur, G., Singh, N., ... Doe, H. (2002) Mixed-micelle formation by strongly interacting surfactant binary mixtures: Effect of head-group modification. *Colloid & Polymer Science*, **280**:990–1000.
- Barai, M., Mandal, M. K., Karak, A., Bordes, R., Patra, A., Dalai, S., & Panda, A. K. (2019) Interfacial and aggregation behavior of dicarboxylic amino acid based surfactants in combination with a cationic surfactant. *Langmuir*, **35**:15306–15314.
- Basu Ray, G., Chakraborty, I., & Moulik, S. P. (2006) Pyrene absorption can be a convenient method for probing critical micellar concentration (cmc) and indexing micellar polarity. *Journal of Colloid and Interface Science*, **294**:248–254.
- Bera, A., Ojha, K., & Mandal, A. (2013) Synergistic effect of mixed surfactant systems on foam behavior and surface tension. *Journal of Surfactants and Detergents*, **16**:621–630.
- Bordes, R., & Holmberg, K. (2011) Physical chemical characteristics of dicarboxylic amino acid-based surfactants. *Colloids and Surfaces, A: Physicochemical and Engineering Aspects*, **391**:32–41.
- Bordes, R., Tropsch, J., & Holmberg, K. (2009) Counterion specificity of surfactants based on dicarboxylic amino acids. *Journal of Colloid and Interface Science*, **338**:529–536.
- Boudier, A., Castagnos, P., Soussan, E., Beaune, G., Belkhef, H., Ménager, C., ... Blanzat, M. (2011) Polyvalent cationic vesicles: Exploring the drug delivery mechanisms. *International Journal of Pharmaceutics*, **403**:230–236.
- Brackman, J. C., & Engberts, J. B. F. N. (1993) Polymer–micelle interactions: Physical organic aspects. *Chemical Society Reviews*, **22**:85–92.
- Butt, H.-J. (1991) Measuring electrostatic, van der Waals, and hydration forces in electrolyte solutions with an atomic force microscope. *Biophysical Journal*, **60**:1438–1444.
- Carpene, P., Aguiar, J., Bernaola-Galván, P., & Camero Ruiz, C. (2002) Problems associated with the treatment of conductivity–concentration data in surfactant solutions: Simulations and experiments. *Langmuir*, **18**:6054–6058.
- Chakraborty, T., & Ghosh, S. (2008) A unified survey of applicability of theories of mixed adsorbed film and mixed micellization. *Journal of Surfactants and Detergents*, **11**:323–334.
- Chen, L., Patrone, N., & Liang, J. F. (2012) Peptide self-assembly on cell membranes to induce cell lysis. *Biomacromolecules*, **13**: 3327–3333.
- Clint, J. H. (1975) Micellization of mixed nonionic surface active agents. *Journal of the Chemical Society, Faraday Transactions*, **71**: 1327–1334.
- Coret, J., Shiloach, A., Berger, P., & Blankschtein, D. (1999) Critical micelle concentrations of ternary surfactant mixtures: Theoretical prediction with user-friendly computer programs and experimental design analysis. *Journal of Surfactants and Detergents*, **2**:51–58.
- Das, S., Ghosh, S., & Das, B. (2018) Formation of mixed micelle in an aqueous mixture of a surface active ionic liquid and a conventional surfactant: Experiment and modeling. *Journal of Chemical & Engineering Data*, **63**:3784–3800.
- Ghosh, S. (2001) Surface chemical and micellar properties of binary and ternary surfactant mixtures (cetyl pyridinium chloride, Tween-40, and Brij-56) in an aqueous medium. *Journal of Colloid and Interface Science*, **244**:128–138.
- Goddard, E. D. (1994) Polymer/surfactant interaction its relevance to detergent systems. *Journal of the American Oil Chemists' Society*, **71**:1–16.
- Gu, B., & Rosen, M. J. (1989) Surface concentrations and molecule interactions in cationic-anionic mixed monolayers at various interfaces. *Journal of Colloid and Interface Science*, **129**:537–553.
- Hao, J., & Hoffmann, H. (2004) Self-assembled structures in excess and salt-free cationic surfactant solutions. *Current Opinion in Colloid & Interface Science*, **9**:279–293.
- Hassan, P. A., Hodgdon, T. K., Sagasaki, M., Fritz-Popovski, G., & Kaler, E. W. (2009) Phase behavior and microstructure evolution in aqueous mixtures of cetyltrimethylammonium bromide and sodium dodecyl tri-oxyethylene sulfate. *Comptes Rendus Chimie*, **12**: 18–29.
- Helbig, C., Baldauf, H., Mahnke, J., Stöckelhuber, K. W., & Schulze, H. J. (1998) Investigation of langmuir monofilms and flotation experiments with anionic/cationic collector mixtures. *International Journal of Mineral Processing*, **53**:135–144.
- Holland, P. M. (1986) Non-ideal mixed micellar solutions. *Advances in Colloid and Interface Science*, **26**:111–129.
- Holland, P. M., & Rubingh, D. N. (1992) Mixed surfactant systems. *American Chemical Society, ACS Symposium Series*. **501**:2–30.
- Huang, J., & Ren, Z. H. (2019) Micellization and interactions for ternary mixtures of amino sulfonate surfactant and nonionic octylphenol polyoxyethylene ethers in aqueous solution: I blending with nonionic surfactants with smaller numbers of hydrophilic unit. *Journal of Molecular Liquids*, **278**:53–60.
- Kronberg, B. (1997) Surfactant mixtures. *Current Opinion in Colloid & Interface Science*, **2**:456–463.
- Kumar, D., Hidayathulla, S., & Rub, M. A. (2018) Association behavior of a mixed system of the antidepressant drug imipramine hydrochloride and dioctyl sulfosuccinate sodium salt: Effect of temperature and salt. *Journal of Molecular Liquids*, **271**:254–264.
- Li, X., & Kunieda, H. (2003) Cationic surfactants: Microemulsion formation and solubilization. *Current Opinion in Colloid & Interface Science*, **8**:327–336.

- Li, F., Li, G.-Z., & Chen, J.-B. (1998) Synergism in mixed zwitterionic-anionic surfactant solutions and the aggregation numbers of the mixed micelles. *Colloids and Surfaces A*, **145**:167–174.
- Li, H. H., Imai, Y., Yamanaka, M., Hayami, Y., Takiue, T., Matsubara, H., & Aratono, M. (2011) Specific counterion effect on the adsorbed film of cationic surfactant mixtures at the air/water interface. *Journal of Colloid and Interface Science*, **359**:189–193.
- Lioi, S. B., Wang, X., Islam, M. R., Danoff, E. J., & English, D. S. (2009) Catanionic surfactant vesicles for electrostatic molecular sequestration and separation. *Physical Chemistry Chemical Physics*, **11**:9315–9325.
- Mahbub, S., Rub, M. A., Hoque, M. A., Khan, M. A., & Kumar, D. (2019) Micellization behavior of cationic and anionic surfactant mixtures at different temperatures: Effect of sodium carbonate and sodium phosphate salts. *Journal of Physical Organic Chemistry*, **39**:67:1–17.
- Maiti, K., Chakraborty, I., Bhattacharya, S. C., Panda, A. K., & Moulik, S. P. (2007) Physicochemical studies of octadecyltrimethylammonium bromide: A critical assessment of its solution behavior with reference to formation of micelle and microemulsion with n-butanol and n-heptane. *The Journal of Physical Chemistry. B*, **111**:14175–14185.
- Manna, K., & Panda, A. K. (2011) Physicochemical studies on the interfacial and micellization behavior of CTAB in aqueous polyethylene glycol media. *Journal of Surfactants and Detergents*, **14**: 563–576.
- Manna, K., Chang, C.-H., & Panda, A. K. (2012) Physicochemical studies on the catanionics of alkyltrimethylammonium bromides and bile salts in aqueous media. *Colloids and Surfaces, A: Physicochemical and Engineering Aspects*, **415**:10–21.
- Mansbach, C. M., Cohen, R. S., & Leff, P. B. (1975) Isolation and properties of the mixed lipid micelles present in intestinal content during fat digestion in man. *The Journal of Clinical Investigation*, **56**:781–791.
- Mao, J., Tian, J., Zhang, W., Yang, X., Zhang, H., Lin, C., ... Zhao, J. (2019) Effects of a counter-ion salt (potassium chloride) on gemini cationic surfactants with different spacer lengths. *Colloids and Surfaces, A: Physicochemical and Engineering Aspects*, **578**:123619.
- Marques, E., Khan, A., da Graca Miguel, M., & Lindman, B. (1993) Self-assembly in mixtures of a cationic and an anionic surfactant: The sodium dodecyl sulfate-didodecyltrimethylammonium bromide-water system. *The Journal of Physical Chemistry*, **97**: 4729–4736.
- Motomura, K., Yamanaka, M., & Aratono, M. (1984) Thermodynamic consideration of the mixed micelle of surfactants. *Colloid & Polymer Science*, **262**:948–955.
- Ohshima, H. (2016) Catanionic surfactants: Novel surrogates of phospholipids. In K. Manna & A. K. Panda (Eds.), *Encyclopedia of Bio-colloid and Biointerface Science* (pp. 1020–1043). New Jersey: John Wiley and Sons.
- Pal, A., & Saini, M. (2019) Aggregation behavior of task-specific acidic ionic liquid n-methyl-2-pyrrolidinium dihydrogen phosphate [nmp][h₂po₄] in aqueous and aqueous salt solutions. *Journal of Surfactants and Detergents*, **22**:491–499.
- Panda, A. K., Sarkar, G., & Manna, K. (2009) Physicochemical studies on surfactant aggregation I. Effect of polyethylene glycols on the micellization of SDS. *Journal of Dispersion Science and Technology*, **30**:1152–1160.
- Patel, U., Parekh, P., Sastry, N. V., Aswal, V. K., & Bahadur, P. (2017) Surface activity, micellization and solubilization of cationic gemini surfactant-conventional surfactants mixed systems. *Journal of Molecular Liquids*, **225**:888–896.
- Peng, F. F. (1996) Surface energy and induction time of fine coals treated with various levels of dispersed collector and their correlation to flotation responses. *Energy & Fuels*, **10**:1202–1207.
- Puvvada, S., & Blankschtein, D. (1992) Theoretical and experimental investigations of micellar properties of aqueous solutions containing binary mixtures of nonionic surfactants. *Journal of Physical Chemistry*, **96**:5579–5592.
- Ray, G. B., Chakraborty, I., & Moulik, S. P. (2005) Self-aggregation of alkyltrimethylammonium bromides (C10-, C12-, C14-, and C16TAB) and their binary mixtures in aqueous medium: A critical and comprehensive assessment of interfacial behavior and bulk properties with reference to two types of micelle formation. *Langmuir*, **21**:10958–10967.
- Ren, Z. H. (2015) Effect of sodium chloride on interaction between amino sulfonate amphoteric surfactant and octylphenol polyoxyethylene ether (10) in aqueous solution. *Journal of Industrial and Engineering Chemistry*, **30**:44–49.
- Ren, Z. H., Huang, J., Luo, Y., Zheng, Y. C., Mei, P., Lai, L., & Chang, Y. L. (2016) Micellization behavior of binary mixtures of amino sulfonate amphoteric surfactant with different octylphenol polyoxyethylene ethers in aqueous salt solution: Both cationic and hydrophilic effects. *Journal of Industrial and Engineering Chemistry*, **36**:263–270.
- Ren, Z. H., Huang, J., Zheng, Y. C., Lai, L., & Hu, L. L. (2017a) Effect of isopropanol on the micellization of binary mixture containing amino sulfonate amphoteric surfactant in aqueous solution: Mixing with octylphenol polyoxyethylene ether. *Journal of Molecular Liquids*, **236**:101–106.
- Ren, Z. H., Huang, J., Zheng, Y. C., Lai, L., & Hu, L. L. (2017b) Interaction and micellar behavior of binary mixture of amino sulfonate amphoteric surfactant with octadecyltrimethylammonium bromide in aqueous solutions of NaCl. *Journal of Chemical & Engineering Data*, **62**:1782–1787.
- Ren, Z. H., Huang, J., Zheng, Y. C., Lai, L., Mei, P., Yu, X. R., & Chang, Y. L. (2018) Micellization and interaction for ternary mixtures of amino sulfonate surfactant and nonionic octylphenol polyoxyethylene ethers in aqueous solution: 2 blending with nonionic surfactant with a longer or shorter hydrophilic chain. *Journal of Molecular Liquids*, **272**:380–386.
- Rosen, M. (1994) Predicting synergism in binary mixtures of surfactants. *Surfactants and Colloids in the Environment*, **95**:39–47.
- Rosen, M. J., & Dahanayake, M. (2000) *Industrial utilization of surfactants, principles and practice* (pp. 28–29). Champaign, IL: AOCSS Press.
- Rosen, M. J., & Hua, X. Y. (1982) Synergism in binary mixtures of surfactants: II. Some experimental data. *Journal of the American Oil Chemists' Society*, **59**:582–585.
- Rosen, M. J., & Kunjappu, J. T. (2012) *Surfactants and interfacial phenomena* (4th ed., p. 616). New York: Wiley.
- Rub, M. A., Azum, N., Khan, F., & Asiri, A. M. (2018) Aggregation of sodium salt of ibuprofen and sodium taurocholate mixture in different media: A tensiometry and fluorometry study. *The Journal of Chemical Thermodynamics*, **121**:199–210.
- Rubingh, D., & Mittal, K. (1979) *Solution chemistry of surfactants* (Vol. 1, p. 337). New York: Plenum.
- Sarmoria, C., Puvvada, S., & Blankschtein, D. (1992) Prediction of critical micelle concentrations of non-ideal binary surfactant mixtures. *Langmuir*, **8**:2690–2697.
- Scamehorn, J. F. (1986) Phenomena in mixed surfactant systems. *ACS Symposium Series*, ISBN13: 9780841209756, **311**:1–198.
- Schulz, E. P., Rodriguez, J., Minardi, R. M., Miraglia, D. B., & Schulz, P. C. (2013) On the applicability of the regular solution theory to multicomponent systems. *Journal of Surfactants and Detergents*, **16**:795–803.
- Sikorska, E., Wyrzykowski, D., Szutkowski, K., Greber, K., Lubecka, E. A., & Zhukov, I. (2016) Thermodynamics, size, and dynamics of zwitterionic dodecylphosphocholine and anionic sodium dodecyl sulfate mixed micelles. *Journal of Thermal Analysis and Calorimetry*, **123**:511–523.

- Sugihara, G., Nagadome, S., Oh, S. W., & Ko, J. S. (2008) A review of recent studies on aqueous binary mixed surfactant systems. *Journal of Oleo Science*, **57**:61–92.
- Tikarha, D., Ghosh, K. K., Quagliotto, P., & Ghosh, S. (2010) Mixed micellization properties of cationic monomeric and gemini surfactants. *Journal of Chemical & Engineering Data*, **55**:4162–4167.
- Upadhyaya, A., Acosta, E. J., Scamhorn, J. F., & Sabatini, D. A. (2007) Adsorption of anionic–cationic surfactant mixtures on metal oxide surfaces. *Journal of Surfactants and Detergents*, **10**: 269–277.
- Vonwandruszka, R. (2005) Mixed surfactant systems, 2nd ed., revised and expanded. volume 124 of the Surfactant Science Series edited by Masahiko Abe (Tokyo University of Science) and John F. Scamhorn (University of Oklahoma) Marcel Dekker, New York. 832, 8247–2150. *Journal of the American Chemical Society*, **127**:9657–9658.
- Wilkinson, J. M., Hipwell, M., Ryan, T., & Avonagh, H. M. A. (2003) Bioactivity of backhousia citriodora: Antibacterial and antifungal activity. *Journal of Agricultural and Food Chemistry*, **51**: 76–81.
- Yingju, F., Zhipeng, L., Le, W., & Jinhua, Z. (2009) Cationic-surfactant-controlled morphosynthesis and gas-sensing properties of corundum-type in 2 O 3. *Nanotechnology*, **20**:285501.



OPEN Micro-structural investigations on oppositely charged mixed surfactant gels with potential dermal applications

Manas Barai¹, Emili Manna², Habiba Sultana¹, Manas Kumar Mandal¹, Kartik Chandra Guchhait³, Tuhin Manna³, Anuttam Patra⁴, Chien-Hsiang Chang⁵, Parikshit Moitra⁶, Chandradipa Ghosh³, Anna-Carin Larsson⁴, Santanu Bhattacharya^{6,7} & Amiya Kumar Panda^{1✉}

Dicarboxylic amino acid-based surfactants (*N*-dodecyl derivatives of -aminomalonate, -aspartate, and -glutamate) in combination with hexadecyltrimethylammonium bromide (HTAB) form a variety of aggregates. Composition and concentration-dependent mixtures exhibit liquid crystal, gel, precipitate, and clear isotropic phases. Liquid crystalline patterns, formed by surfactant mixtures, were identified by polarizing optical microscopy. FE-SEM studies reveal the existence of surface morphologies of different mixed aggregates. Phase transition and associated weight loss were found to depend on the composition where thermotropic behaviours were revealed through combined differential scanning calorimetry and thermogravimetric studies. Systems comprising more than 60 mol% HTAB demonstrate shear-thinning behaviour. Gels cause insignificant toxicity to human peripheral lymphocytes and irritation to bare mouse skin; they do not display the symptoms of cutaneous irritation, neutrophilic invasion, and inflammation (erythema, edema, and skin thinning) as evidenced by cumulative irritancy index score. Gels also exhibit substantial antibacterial effects on *Staphylococcus aureus*, a potent causative agent of skin and soft tissue infections, suggesting its possible application as a vehicle for topical dermatological drug delivery.

Formation of gels and different liquid crystalline phases by oppositely charged mixed surfactant systems depend on the composition, surfactant chain length, salinity, temperature, pH and external field, etc.^{1–5}. Artificial gels possess regulated super-structure^{6–10}, where the properties of the fabricated liquid crystals depend on electrostatic, hydrogen bond, hydrophobic, and van der Waals interactions among the components^{11–13}. Gels are associated with two independent transitions, viz., the sol–gel transition of the gelator and anisotropic–isotropic transition of the liquid crystals^{9,10,14–18}. Gelatinous property, structure, and shape of surfactant aggregates largely depend on the molecular architecture of the aggregating species^{14,19,20}.

Gels have versatile applications in tissue engineering²¹, hemostasis bandages^{22–26}, photo-patterning^{17,27–30}, 3D-printing^{31,32}, electrochemistry³³, pharmaceutical formulation^{5,34–36}, and regenerative medicine^{10,37–39}, etc. Recent advances in the design and synthesis of dicarboxylic amino acid-based surfactants (AAS) have opened up their wide range of applications as chelator in metal extraction⁴⁰. Due to its “green nature”, aggregation behaviour of AAS in combination with HTAB have been studied in detail where some mixed surfactants can form gel¹⁶. This has encouraged the present research group to undertake further investigations on such aggregates at higher concentrations to explore the possibility of using those for topical dermatological drug delivery.

The main aim of the present work is to undertake physicochemical investigations on different types of aggregates formed by AAS + HTAB. While HTAB shows antimicrobial activities, AASs are biocompatible⁴¹. Because

¹Department of Chemistry, Vidyasagar University, Midnapore 721102, West Bengal, India. ²Centre for Life Sciences, Vidyasagar University, Midnapore 721102, West Bengal, India. ³Department of Human Physiology, Vidyasagar University, Midnapore 721102, West Bengal, India. ⁴Chemistry of Interfaces Group, Luleå University of Technology, 97187 Luleå, Sweden. ⁵Department of Chemical Engineering, National Cheng Kung University, Tainan, Taiwan. ⁶India and School of Applied & interdisciplinary Sciences, Indian Association for the Cultivation of Science, Kolkata 700032, India. ⁷Department of Organic Chemistry, Indian Institute of Science, Bangalore 560012, Karnataka, India. ✉email: akpanda@mail.vidyasagar.ac.in

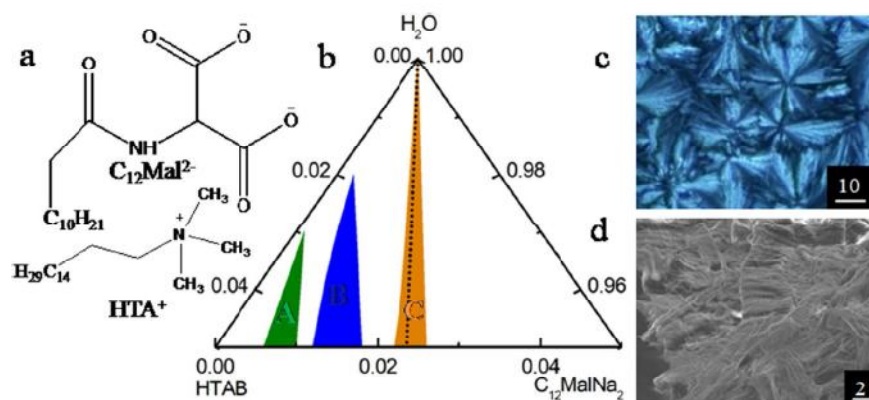


Figure 1. (a) Chemical structure of $C_{12}Mal^{2-}$ and HTA^+ ; (b) truncated phase diagram of $C_{12}MalNa_2 + HTAB + water$ mixed system at 25 °C. Phases: (A), gel; (B), viscous; (C), precipitate; and clear region indicate the formation of micelle. The dotted line in panel b corresponds to equimolar region. Panel (c), POM and (d), FE-SEM image of 5 wt% $C_{12}MalNa_2 + HTAB$ (40:60, w/w) gel respectively. Scale bars (in μm) are mentioned in the microscopic images.

of its toxicity, individual use of HTAB is unwarranted. It is believed that, when HTAB is used in combination with AASs, its toxicity will be substantially reduced^{42,43}. To check the biocompatibility of gels and their possible dermatological application in the topical form, cytotoxicity, skin irritation, and histological studies were carried out. HTAB is known to have antimicrobial activities⁴², for which antibacterial activities of AAS + HTAB mixtures are considered to be worth investigating. Hence, antibacterial activities of the gels on *Staphylococcus aureus*, one of the causative agents for persistent skin and soft tissue infections, were also explored.

Results and discussion

Structures of $C_{12}MalNa_2$ and HTAB are shown in (Fig. 1a) along with other information. Manifestation on the Gibbs ternary phase diagram (Fig. 1b) demonstrates the occurrence of gel, viscous, precipitate and clear fluid states. With increasing proportion of HTAB, surfactant mixtures form gels where the relative proportion of viscous and gel states increase following the order: $C_{12}MalNa_2 + HTAB > C_{12}AspNa_2 + HTAB > C_{12}GluNa_2 + HTAB$ (Fig. S1, supplementary section). Hydrophobic interaction between AASs and HTAB is the predominant factor for the formation of different types of aggregates besides the electrostatic attraction⁸. AASs interact with HTAB at a 1:2 mol ratio and form gels at equimolar region due to the dominance of the HTAB molecules⁴⁴. Microstructural investigations on surfactant mixtures at different concentrations (AAS + HTAB) and different compositions (AAS/HTAB) were further investigated through polarizing optical microscopy (POM) and field emission scanning electron microscopic (FE-SEM) studies. POM studies reveal the occurrence of liquid crystal and associated textures as shown in Fig. 1c. Gels exhibit different textures in the surfactant concentration range of 3–5 wt%. With increasing proportions of HTAB, $C_{12}MalNa_2 + HTAB$ gels display nematic, smectic, spherulite, cholesteric, calamitic, and flower-like textures (Fig. S2, Table S1A)^{44–47}. Nematic liquid textures originate from thread-like shapes, that correspond to surfactant gels aligning themselves in threadlike shapes as reported earlier⁴⁸. The patterns become more complex with enhanced sizes due to the aggregation and associative interactions between AASs and HTAB. Texture size increases with increasing proportions of HTAB, which has a higher cross-sectional area than the AASs⁴⁹.

Features become more prominent with increasing mixed surfactant concentrations, common in the case of lyotropic liquid crystals^{16,47} (Fig. S2, Supplementary Section). In the case of $C_{12}AspNa_2 + HTAB$ gels for 50, 60, and 80 wt% of HTAB, smectic (Fig. S3a₁), spherulite (Fig. S3b₁), and flower-like (Fig. S3c₁) patterns are observed^{50,51}, while in the case of $C_{12}GluNa_2 + HTAB$ mixtures, discotic (Fig. S3a₂), calamitic (Fig. S3b₂), and flower-like (Fig. S3c₂, Table S1B) textures are observed due to the formation of sterically favourable seven and eight-member rings. Two carboxylate groups get progressively separated by one methylene group while moving from $C_{12}MalNa_2$ to $C_{12}AspNa_2$ to $C_{12}GluNa_2$. Accordingly, two carboxylate groups of AASs can electrostatically interact with one HTAB to form six, seven, and eight-member rings⁴⁹. Smectic textures designate ordered and rigid layer structure whereby $C_{12}MalNa_2 + HTAB$ can closely interact with HTAB to exhibit smectic textures (Fig. S2b_{1,2,3,4,5,6,7,8}). The nematic texture (Fig. S2a_{1,2,3,4,5,6,7,8}), is characteristic of stacked layer and positional order whereby the discotic texture (Fig. S2b₁) is due to rigid disk-like core, according to Fan Shao et al.^{52,53}. Spherulite textures (Fig. S2a_{5,6,7,8}) are larger bundles and the hexagonal shapes caused by close packing are even more defined, as also reported by Haas et al.⁵⁴ $C_{12}MalNa_2 + HTAB$ gels display a more prominent spherulite texture (Fig. S2a_{5,6,7,8}) than $C_{12}AspNa_2 + HTAB$ due to the formation of strongly aggregated structure and associative interaction with HTAB. Calamitic textures, exhibited by $C_{12}GluNa_2 + HTAB$ gels (Fig. S3b₂, Table S1B) have a relatively flexible core, due to weak hydrophobic interaction between the oppositely charged $C_{12}GluNa_2$ and HTAB system.

Microstructures of the aggregates were further investigated with FE-SEM studies, which display interconnected morphologies (Fig. 1d)^{27,55,56}. To achieve optimal solvation and swelling, the pore of the gels can provide

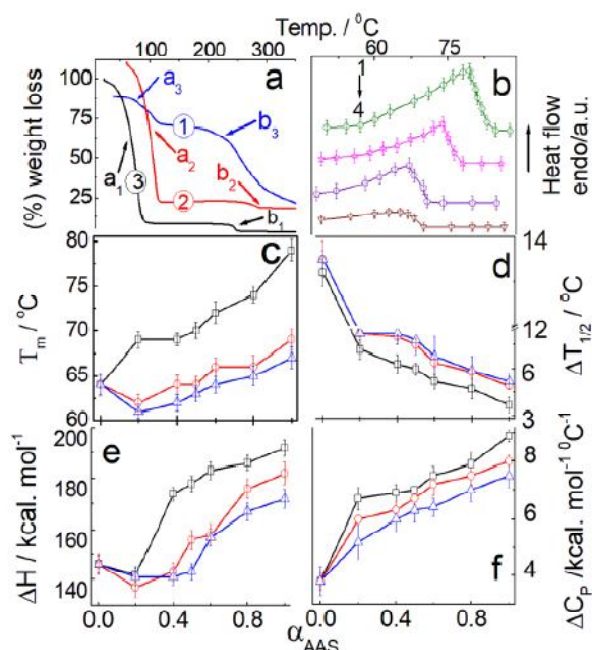


Figure 2. (a) TGA of AAS+HTAB (100 mM, 40/60, M/M) gel. Systems: 1, $C_{12}GluNa_2$ +HTAB; 2, $C_{12}AspNa_2$ +HTAB and 3, $C_{12}MalNa_2$ +HTAB. $a_1, b_1, a_2, b_2, a_3,$ and b_3 represent different phase transitions. (b) DSC of $C_{12}MalNa_2$ +HTAB mixture at different mole% of $C_{12}MalNa_2$: 1, 80; 2, 60; 3, 40 and 4, 0. Variations of (c) chain melting temperature (T_m); (d) half peak height ($\Delta T_{1/2}$); (e) enthalpy change (ΔH) and (f) heat capacity change (ΔC_p) with the mole fraction of AAS (α_{AAS}). The line colours in panels (c–f) represent similar surfactant composition as in panel (a). Scan rate: $2\text{ }^\circ\text{C min}^{-1}$.

pockets for water molecules, necessary for hydration, to be included by surface tension. $C_{12}MalNa_2$, in combination with HTAB, shows flower-like (Fig. S4e₁,b₄,b₅,c₅,e₅ and Table S1A), coral-like (Fig. S4a₁,d₂), and porous—(Fig. S4a₃) architectures due to the existence of protrusions and larger channels⁵⁷. Flake—(Fig. S4c₁,b₃,c₄), leaf—(Fig. S4b₁,d₁,a₂), leaf+flake—(Fig. S4b₂), wrinkled—(Fig. S4a₅), and sheet-like structures (Fig. S4d₃) display extended flat features. Fibrous texture (Fig. S4c₃ and d₃) indicate larger bundled-fibre network structure. Granular—(Fig. S4e₂,e₄) and cuboid (Fig. S4e₃) morphologies were observed in some cases. Irregular structure (Fig. S4c₂) and amorphous materials (Fig. S4a₄,d₄) had also been observed, in which cases the aggregates do not have any particular features. In the cases of $C_{12}AspNa_2$ +HTAB gels with 50, 60, and 80 wt% of HTAB exhibits fibrous, dense fibrous (Fig. S5a₁,b₁, and Table S1B) and densely-packed cuboid structures (Fig. S5c₁). $C_{12}GluNa_2$ +HTAB mixtures exhibit cuboid (Fig. S5a₂), irregular structures (Fig. S5b₂), and sheet-like structures (Fig. S5c₂)^{27,28,57–59}. $C_{12}AspNa_2$ +HTAB and $C_{12}GluNa_2$ +HTAB gels show characteristic cuboid structures (Fig. S5c₁,a₂) due to the emergence of micropores at the surface of gels⁶⁰. $C_{12}AspNa_2$ +HTAB gels have fibre network-like morphologies (Fig. S5a₁,b₁) that can hold water molecules due to assisted surface tension enhancement. Irregular (Fig. S5b₂) and sheet-like structures (Fig. S5c₂) for $C_{12}GluNa_2$ +HTAB indicate the entrapment of water molecules into the gels. Maximum number of HTAB accumulated in gels indicate that HTAB plays a fundamental role in demonstrating higher aggregation and formation of porous-like morphology, which are in consonance with the phase manifestation, and POM studies.

Phase transition and associated weight loss of gels were investigated by thermogravimetry analysis (TGA)^{61–63}. Results on the TGA of the pure components, as well as AAS+HTAB aggregates, have been summarized in Fig. S6 and Table S2. HTAB decomposes to produce some solid carbon along with the production of long-chain hydrocarbon, nitrogen, and hydrogen^{61,64}, whereby decomposition of $C_{12}MalNa_2$, $C_{12}AspNa_2$, and $C_{12}GluNa_2$ to produce dodecane (or smaller alkyl fragments) and free aminomalonic, aspartic, and glutamic acid⁶³. AAS+HTAB gels show endothermic peaks in the temperature range of 40 to 100 °C due to dehydration (Fig. 2a)⁶⁵. Two carboxylate groups of $C_{12}MalNa_2$ electrostatically interact with HTAB that result in higher ionicity and subsequent moisture absorption capability than $C_{12}AspNa_2$ and $C_{12}GluNa_2$. In the case of $C_{12}GluNa_2$, two ionic carboxylate groups are separated by three methylene groups; so its interaction capability with HTAB and magnitude of hydration is lower. Formation of rigid aggregates result in the higher chain melting temperature (T_m) as determined from the DSC studies.

Thermotropic behaviour and associated parameters were evaluated by DSC studies⁴⁴. Variation of phase transition temperature (T_m), width at half peak height ($\Delta T_{1/2}$), enthalpy change (ΔH) and corresponding heat capacity changes (ΔC_p) were determined as functions of α_{AAS} as summarized in (Fig. 2). HTAB exhibits two endothermic peaks at 64 °C and 84 °C indicating transition from solid to liquid crystalline phase and the phenomenon

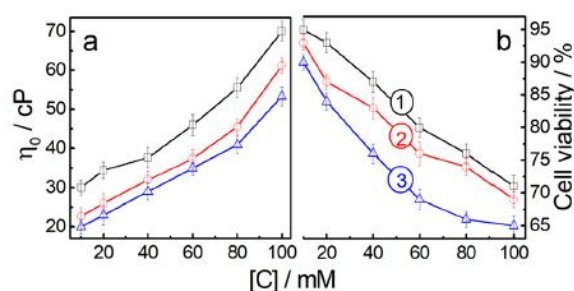


Figure 3. Variation of a, zero shear viscosity and b, human blood lymphocyte cell viability with AASs + HTAB (2/3, M/M) mixed surfactant concentration [C]. Systems: 1, $C_{12}MalNa_2$ + HTAB; 2, $C_{12}AspNa_2$ + HTAB and 3, $C_{12}GluNa_2$ + HTAB.

of dehydration⁴⁴, common in the amphiphiles (Fig. 2b)⁶³. With increasing α_{AAS} , T_m values increase due to the incorporation of HTAB in the aggregates and assimilation of HTAB with AASs; relatively sharp peaks indicate favourable hydrocarbon chain packing (Fig. 2c)⁴⁹. Lowering of T_m is due to size reduction, decreased specific surface area, and interaction between oppositely charged surfactants also known as Kelvin effect⁶⁶. Widening of the melting peaks designates multi-crystallinity and heterogeneity⁶⁶. The extent of hydrophobic interaction between AAS and HTAB is lower in $C_{12}AspNa_2$ and $C_{12}GluNa_2$, where the T_m values follow the sequence: $C_{12}MalNa_2$ + HTAB > $C_{12}AspNa_2$ + HTAB > $C_{12}GluNa_2$ + HTAB. With increasing α_{AAS} , $\Delta T_{1/2}$ values decrease indicating better packing of the hydrophilic overlayer as well as oppositely charged head groups (Fig. 2d). With increasing associative interaction between AAS and HTAB increased crystal imperfection results in higher $\Delta T_{1/2}$ values. Increasing magnitude of interaction with increasing proportion of HTAB induces the formation of ion-pair amphiphiles, resulting in higher ΔH values for the surfactant mixtures (Fig. 2e). With increasing α_{AAS} , ΔCp values gradually increase and exhibit endothermicity due to the formation of water overlayer around surfactant aggregates (Fig. 2f). Lower values of ΔCp are due to the increase in multicrystallinity.

Viscosity studies on AAS + HTAB mixtures at different combinations exhibit shear-thinning (results not shown)⁴⁹. Zero shear viscosity (η_0) vs. concentration profile for the gels comprising 60 mol% HTAB are shown in Fig. 3a.

With increasing surfactant concentrations, viscosity increases monotonously in the range of 10 to 100 mM. The sequence in the viscosity variation follows the order: $C_{12}MalNa_2$ + HTAB > $C_{12}AspNa_2$ + HTAB > $C_{12}GluNa_2$ + HTAB, which are in consonance with the previous studies. Due to the stronger packing and subsequent formation of rigid-structured aggregates, the viscosity of $C_{12}MalNa_2$ + HTAB system is higher than the other two.

AAS + HTAB aggregates exhibit less toxicity against human blood lymphocyte up to 20 mM; although, cytotoxicity increases with increasing surfactant concentration (Fig. 3b). Results suggest that cytotoxicities are in consonance with the corresponding viscosity of the system.

Dermal responses towards the gels were assessed through topical application of the experimental gels on the bare mice skin surface where sterile distilled water and 5% (w/v) phenol-water were used as a negative (NC) and positive control (PC), respectively. Dermal irritability, as evidenced by the development of edema, and erythema were tested carefully and were scored according to the Organization for Economic Co-operation and Development (OECD) guidelines (Fig. 4A,C).

Simultaneously, developments of skin inflammation upon the application of gels were studied histologically by examining the hematoxylin-eosinY stained gel-treated skins for neutrophil invasion (Fig. 4B)^{68,69}. It was found that gels do not induce symptoms related to skin irritation and inflammation (erythema, edema, and neutrophilic invasion) as shown in Fig. 4A(ii),B(ii). Effects of gels on mice skin appeared similar to the effect of sterile distilled water, used as negative control (NC). On the other hand, 5% (w/v) phenol-water (PC) caused considerable erythema, edema, and neutrophilic invasion Fig. 4A(iii),B(iii), resulting in high CII score (> 5.00) that corresponds to moderate skin irritation⁶⁷. The CII score, for each of the gel treatment, was calculated to be as low as < 0.49 (Fig. 4C). These values, along with the CII values observed in NC group, correspond to the scores representing no potential skin irritation according to the OECD guidelines⁶⁷. Besides, mice treated with 5% (w/v) phenol-water (PC group) visibly suffered from post-treatment erythema and edema resulting in higher CII score (> 5.00) that corresponds to moderate skin irritation⁶⁷. Similarly, Fig. 4C reveals that there were significant differences ($P < 0.05$) in CII scores between 5% (w/v) phenol-water-treated group and each of the gel-treated groups. Based on these findings, it could be concluded that gels used in this study do not have significant skin irritation potential and thus may safely be used for topical dermal applications.

Gels also exhibited substantial antibacterial activities against *Staphylococcus aureus*, a gram-positive pathogenic bacteria. In spite of ~90% lymphocyte viability, 20 mM surfactant mixtures of AAS + HTAB (40:60, M/M) could substantially inhibit bacterial growth⁶⁷. The minimum inhibitory concentration (MIC) is the lowest concentration of a substance that renders no turbidity in bacterial culture, corresponding to 99% bacterial growth inhibition⁷⁰. The MIC value of individual surfactant mixture was determined for different clinical isolates of *S. aureus*, i.e., American Type Culture Collection (ATCC) 25923 and four other clinical isolates: AK1, AK2, AK8, and AK10 with the broth dilution method. Vancomycin was also used as a reference drug for growth

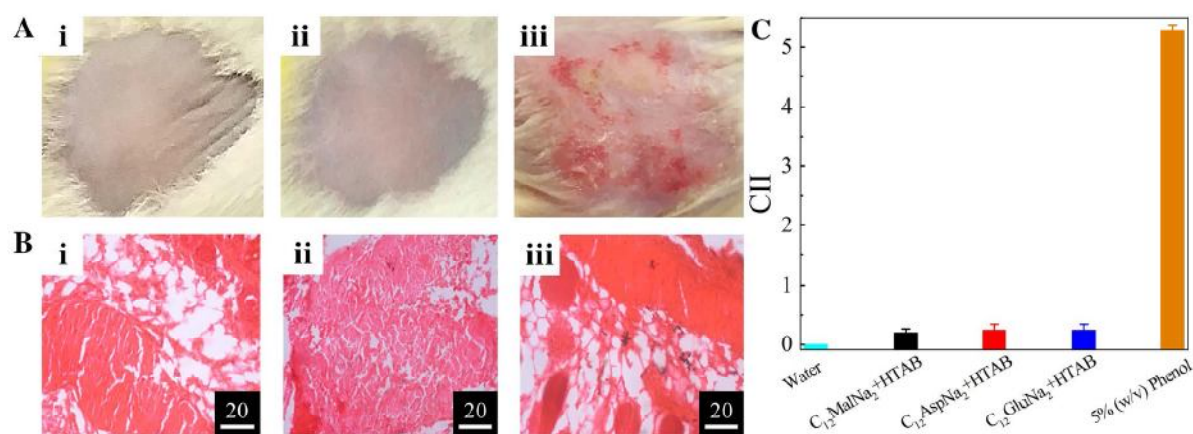


Figure 4. Effects of AAS+HTAB gels on mice skin. Gels were applied at the dorsal area of the trunk region of swiss albino mice for seven consecutive days and the effects recorded are presented through (A) photographs of treated skins and (B) corresponding histopathological evaluation of inflammation through micrographs. Systems: i, sterile distilled water (NC); ii, C₁₂MalNa₂+HTAB gel (100 mM, 60/40, M/M) and iii, 5% (w/v) phenol-water (PC). Micrographic scale bar: 20 μm. (C) cumulative irritancy index (CII) scores for skins treated with different systems, calculated according to Organization for Economic Co-operation and Development (OECD) guidelines⁶⁷. Overall comparison of CII scores among the groups were carried out by the Kruskal–Wallis test followed by post-hoc Dunn’s test for multiple comparisons between each pair of groups. Significant differences in CII scores at $P < 0.05$ were obtained between groups PC vs. NC, PC vs. C₁₂MalNa₂+HTAB, PC vs. C₁₂AspNa₂+HTAB, and PC vs. C₁₂GluNa₂+HTAB gels.

<i>S. aureus</i> strains	MIC (μM) ^a			
	Vancomycin	C ₁₂ MalNa ₂ +HTAB	C ₁₂ AspNa ₂ +HTAB	C ₁₂ GluNa ₂ +HTAB
AK1	0.827	20	40	20
AK2	1.242	40	60	40
AK8	1.035	40	50	40
AK0	0.827	30	40	30
ATCC 25923	0.482	10	20	10

Table 1. Antibacterial activities of AAS+HTAB gels against *S. aureus* clinical isolates. ^aFor the determination of MIC value, serial concentrations in the range of 5 to 100 μM (with an increment of 5 μM in each step) of each surfactant mixture was applied to bacterial culture containing 1×10^7 CFU. Data represent mean values of three experimental outcomes.

inhibition^{71,72} as it is a widely used effective ‘drug of choice’ against *S. aureus* infections⁷³. With the MIC value in the range of 10–40 μM, C₁₂MalNa₂+HTAB and C₁₂GluNa₂+HTAB gels exhibited higher antibacterial activities than C₁₂AspNa₂+HTAB, with the MIC value in the range of 20–60 μM, as summarized in Table 1.

Results indicate that gels can potentially be used in the treatment of bacteria-borne dermatological infections. In addition, the gels are expected to exhibit higher entrapment efficiency and sustained release of dermatological drugs in terms of topical applications. However, further in vitro and in vivo studies are warranted to substantiate the aptitude of the gels as potential drug delivery systems. Besides, studies involving composition structure and functional correlations are also considered to be worthy.

Summary and conclusions

Microstructures of AAS+HTAB aggregates were investigated by combined phase manifestation, polarizing optical microscopy and field-emission scanning electron microscopic studies. Texture of liquid crystals depended on the concentration and proportion of constituent surfactants. Energetics of phase transition processes were evaluated by TGA and DSC studies. Cytotoxicity could be correlated with the viscosity of the gels. Gels impart insignificant skin irritation although they possess substantial antibacterial activities that project their potential as dermal drug delivery systems. However further in vitro and in vivo studies by incorporating appropriate drugs into the gels are necessary and is considered as the future perspectives.

In order to draw final conclusions about solvation, water channels, and pores, drawn from the morphological studies, further characterization techniques, viz., small-angle X-ray scattering and small-angle neutron scattering studies, combined with the molecular dynamics simulation studies are worthy to be investigated. These are considered as the future perspectives.

Experimental section

Materials. Hexadecyltrimethylammonium bromide (HTAB), fetal bovine serum (FBS) and histopaque-1077[™] were the products from Sigma-Aldrich Chemicals Pvt. Ltd. (USA). Disodium salts of AAS were synthesized according to the previous reports⁷⁴. Phenol, hematoxylin, eosin Y, and 3-(4, 5-dimethylthiazol-2-yl)-2, 5-diphenyl tetrazolium bromide (MTT) were purchased from Hi Media Laboratories Pvt. Ltd. India. Double distilled water was used throughout the experiments. All the chemicals were stated to be $\geq 99\%$ pure and were used as received.

Methods. Phase manifestation. Composition, close to the boundary of the two-phase regions, was detected by homogeneous mixing of aqueous stock solution of oppositely charged surfactants at 25 °C. The exact boundary of the two-phase region was detected by further step wise addition (using a calibrated micropipette under constant stirring) of a higher concentration of AASs into the HTAB solution. On the basis of visual observation, more than one hundred samples were collected at different AASs and HTAB weight ratios and phase boundaries were identified⁷⁵. The different phases were recorded consecutively for a longer time-period (upto fifteen days, after which the samples started microbial degradation). All the experiments were repeated thrice to ensure reproducibility.

Microscopic studies. The texture of different combinations of the mixed surfactant systems were recorded with a polarizing optical microscope (POM, Nikon ECLIPSELV100POL, Japan) set with a CCD camera. The sample was placed onto a glass slide and thereafter the POM images were recorded. Morphology of the surfactant aggregates were investigated with field emission-scanning electron microscopy (FE-SEM, ZEISS EVO 18, Germany). Samples were prepared by the drop-casting of the gel on a freshly cleaved mica foil and kept in air for two hours for solvent evaporation. Those were further dried at reduced pressure for two hours. The gold-sputtered samples were then analysed in FE-SEM at the operating voltage of 20–30 kV.

Thermogravimetric analysis (TGA). Weight loss and thermal stability of the gels were investigated by TGA, performed using Pyris 6 TGA-DTA-8000 (Perkin Elmer, USA). Samples were scanned in the temperature range of 50–500 °C with a scan rate of 2 °C min⁻¹ under nitrogen gas flowing conditions.

Differential scanning calorimetric (DSC) studies. DSC studies were performed to evaluate the chain melting temperature (T_m) and associated thermodynamic parameters of mixed surfactant systems that control its physical states. DSC measurements were recorded using a Pyris 6 DSC-8000 (Perkin Elmer, USA) differential scanning calorimeter with indium as a calibrator before performing the experiment. After equilibrating for 10 min, the sample was scanned in the temperature range 0–100 °C with a scan rate of 2 °C min⁻¹ during the heating cycle. From the thermogram the peak temperature and enthalpy of phase transition were evaluated. Endothermic peak vs. temperature in evaluating different physicochemical parameters of mixed surfactant system were considered⁷⁶.

Rheology studies. Viscosities of different surfactant mixtures were determined with a DV II-Pro rotoviscometer (Brookfield, USA) with a stated accuracy of ± 0.01 cP. 1.0 mL surfactant solution of different concentrations (40, 60, 80, and 100 mm) were taken in a cone and plate type rotoviscometer separately⁷⁷. Viscosities were measured at different shear rates (ranging from 76 to 380 s⁻¹). Zero shear viscosity (η_0) was determined from the intercept of the plot of viscosity vs. shear rate by fitting polynomial regression. Temperature during the viscosity measurement was controlled by a circulatory water bath MIC-255 (Hanntech Corporation, South Korea).

Biological activities. All the biological experiments were performed in accordance with relevant guidelines and regulations, duly approved by the Institutional Ethics Committee, Vidyasagar University. All the methods were carried out in accordance with relevant guidelines and regulations.

Cytotoxicity studies. Cytotoxicity studies were carried out following the method of Sun et al.⁶⁷ 5 mL of human blood (volunteered by healthy persons) was diluted (1:1) with phosphate-buffered saline (PBS) and added to Histopaque-1077. Informed consent was obtained from all subjects. It was centrifuged at 1500 rpm for 40 min at the room temperature. The upper layer containing lymphocytes was further washed through centrifugation. Lymphocytes were re-suspended in Roswell Park Memorial Institute (RPMI) complete media supplemented with 10% (w/v) FBS and incubated for a day at 37 °C in 5% (v/v) CO₂ environment (in CO₂ incubator)⁷⁸. Cytotoxicity of selected gels were estimated with MTT assay⁷⁹. 20 μ L 5% (w/v) MTT solution was added to each well of the microtitre plate, having RPMI-suspended lymphocytes with or without the gels. Then the plate was incubated at 37 °C for 4 h in metabolizing MTT to formazan. After the aspiration of the supernatant, 100 μ L HCl+isopropanoic acid solution (1:1) was added to each well of the culture plate and mixed to dissolve the formazan crystals. Optical density (OD) of the sample was measured on an ELISA reader (Model 550, BIO-RAD, USA) using test and reference wavelengths of 570 and 630 nm, respectively. Percentage of cell viability was calculated using the following equation⁷⁹:

$$\text{Cell viability \%} = \left[\frac{\text{OD}_{\text{sample}} - \text{OD}_{\text{control}}}{\text{OD}_{\text{control}}} \right] \times 100 \quad (1)$$

Skin irritation test. The biocompatibility of the experimental gels (AAS+HTAB) were investigated through skin irritation tests on swiss albino mice, in compliance with the Animal Research: Reporting of in vivo Experiments (ARRIVE) guidelines⁸⁰. The tests were performed following the method mentioned in the Good Laboratory Practice Standards (GLPS) manual and the guidelines of OECD for acute dermal irritation⁸¹. Thirty healthy swiss albino mice were divided into five groups, each group consisting of six mice. Group A was negative control (NC, treated with sterile distilled water) and group E was positive control (PC, treated with 5% (w/v) phenol-water). Mice of group C, D, and E were treated individually with 100 mM C₁₂MalNa₂+HTAB, C₁₂AspNa₂+HTAB and C₁₂GluNa₂+HTAB gels, respectively. Prior to the application of gels, hairs of the dorsal area of the trunk region of all mice were removed followed by the topical application of 500 μ L of the gels and the controls, respectively. After 1 h, signs of erythema or edema in individual animal was recorded. The entire procedure of dermal application of gels and subsequent recording for any irritation was continued for seven consecutive days. The CII score for each of the treated groups were calculated according to OECD guidelines⁸¹. CII score of each treated group is the average score, i.e., score of a total of erythema and edema divided by the number of animals and testing days.

Histological studies of mice skin. Animals were sacrificed post euthanasia by carbon dioxide asphyxiation after the completion of skin treatment with gels and controls for seven consecutive days. The treated skins were processed in wax blocks and transverse sections were prepared, followed by staining with hematoxylin-eosinY (HE)⁸². The prepared skin sections were further examined under a light microscope (Axioscope A1; Carl Zeiss, Germany). Histology of the gel-treated skins were compared with the controls.

Studies on antibacterial activity. Antibacterial efficacies of the gels against the gram-positive bacterial pathogen, *Staphylococcus aureus*, grown in Luria Bertani (LB) broth, were evaluated. MIC of each gel against the five clinical isolates of *S. aureus* (AK1, AK2, AK8 and AK10 along with ATCC 25923) was determined by broth dilution method. 10 μ L gelatinous suspension of surfactant mixture at particular composition was added to 1 mL bacterial culture in LB having approximately 1×10^7 CFU. Each surfactant mixture (AAS+HTAB) was added to the bacterial culture in the concentration range of 5 to 100 μ M (with an increment of 5 μ M in each step) in a serial manner for individual bacteria and were incubated at 37 °C for 18 h^{70–72,82}. Vancomycin was used as reference drug for growth inhibition. All the experiments were repeated thrice.

Statistical analysis. The mean value and standard deviation of the quantitative variables were calculated after repeating each quantification three times. Overall comparisons of data among the groups were carried out by the Kruskal–Wallis test. This was followed by post hoc Dunn's test for multiple comparisons of data between each pair of groups. Differences were considered significant at $P < 0.05$ ⁸³.

Received: 13 January 2021; Accepted: 16 June 2021

Published online: 30 July 2021

References

1. Fanasca, S. *et al.* Changes in antioxidant content of tomato fruits in response to cultivar and nutrient solution composition. *J. Agric. Food Chem.* **54**, 4319–4325 (2006).
2. Lopez-Leon, T., Fernandez-Nieves, A., Nobili, M. & Blanc, C. Nematic-smectic transition in spherical shells. *Phys. Rev. Lett.* **106**, 247802–247809 (2011).
3. Pelton, R. Temperature-sensitive aqueous microgels. *Adv. Colloid Interface Sci.* **85**, 1–33 (2000).
4. Saunders, B. R. & Vincent, B. Microgel particles as model colloids: theory, properties and applications. *Adv. Colloid Interface Sci.* **80**, 1–25 (1999).
5. Williams, R. J. *et al.* Enzyme-assisted self-assembly under thermodynamic control. *Nat. Nanotechnol.* **4**, 19–25 (2009).
6. Barker, C. A., Saul, D., Tiddy, G. J. T., Wheeler, B. A. & Willis, E. Phase structure, nuclear magnetic resonance and rheological properties of viscoelastic sodium dodecyl sulphate and trimethylammonium bromide mixtures. *J. Chem. Soc. Faraday. Trans. 1* (70), 154–162 (1974).
7. Hammer, S. E., Fbert, M. & Weinbruch, S. Comparison of operator- and computer-controlled scanning electron microscopy of particles from different atmospheric aerosol types. *Anal. Bioanal. Chem.* **411**, 1633–1645 (2019).
8. Herrington, K. L., Kaler, E. W., Miller, D. D., Zasadzinski, J. A. & Chiruvolu, S. Phase behavior of aqueous mixtures of dodecyltrimethylammonium bromide (DTAB) and sodium dodecyl sulfate (SDS). *J. Phys. Chem.* **97**, 13792–13802 (1993).
9. Jokela, P., Jönsson, B. & Wennerström, H. Phase equilibria in systems containing both an anionic and a cationic amphiphile: A thermodynamic model calculation. *Surf. Ads. Surf. Spectr. Disp. Sys.* **235**, 17–22 (1985).
10. Sangeetha, N. M. & Maitra, U. Supramolecular gels: Functions and uses. *Chem. Soc. Rev.* **34**, 821–836 (2005).
11. Ohshima, H. (ed.) *Cationic Surfactants: Novel Surrogates of Phospholipids* Vol. 1 (Wiley, 2016).
12. Holland, P. M. & Rubingh, D. N. Mixed surfactant systems, in mixed surfactant systems. *Am. Chem. Soc.* **114**, 2–30 (1992).
13. Kronberg, B. Surfactant mixtures. *Cur. Opin. Colloid Interface Sci.* **2**, 456–463 (1997).
14. Du, X., Zhou, J., Shi, J. & Xu, B. Supramolecular hydrogelators and hydrogels: From soft matter to molecular biomaterials. *Chem. Rev.* **115**, 13165–13307 (2015).
15. Hirst, A. R., Escuder, B., Miravet, J. F. & Smith, D. K. High-tech applications of self-assembling supramolecular nanostructured gel-phase materials: From regenerative medicine to electronic devices. *Angew. Chem.* **47**, 8002–8018 (2008).
16. Kato, T., Hirai, Y., Nakaso, S. & Moriyama, M. Liquid-crystalline physical gels. *Chem. Soc. Rev.* **36**, 1857–1867 (2007).
17. Matsumoto, S. *et al.* Photo gel–sol/sol–gel transition and its patterning of a supramolecular hydrogel as stimulated responsive biomaterials. *Chem. Eur. J.* **14**, 3977–3986 (2008).
18. Mizoshita, N., Kutsuna, T., Kato, T. & Hanabusa, K. Smectic liquid-crystalline physical gels: Anisotropic self-aggregation of hydrogen-bonded molecules in layered structures. *Chem. Commun.* **12**, 781–782 (1999).

19. Karsai, Á., Murvai, Ú., Soós, K., Penke, B. & Kellermyer, M. S. Oriented epitaxial growth of amyloid fibrils of the N27C mutant β 25–35 peptide. *Eur. Biophys. J.* **37**, 1133–1137 (2008).
20. Li, Z. *et al.* Observation of exchange bias in the martensitic state of $\text{Ni}_{50}\text{Mn}_{30}\text{Sn}_{14}$ Heusler alloy. *Appl. Phys. Lett.* **91**, 112505 (2007).
21. Chivers, P. R. & Smith, D. K. Shaping and structuring supramolecular gels. *Nat. Rev. Mater.* **4**, 463–478 (2019).
22. Ding, R. *et al.* Hybrid photosensitizer based on amphiphilic block copolymer stabilized silver nanoparticles for highly efficient photodynamic inactivation of bacteria. *RSC Adv.* **6**, 20392–20398 (2016).
23. Krall, A. H. & Weitz, D. A. Internal dynamics and elasticity of fractal colloidal gels. *Phys. Rev. Lett.* **80**, 778–781 (1998).
24. Li, L. *et al.* A nanostructured conductive hydrogels-based biosensor platform for human metabolite detection. *Nano Lett.* **15**, 1146–1151 (2015).
25. Pan, L. *et al.* Hierarchical nanostructured conducting polymer hydrogel with high electrochemical activity. *Proc. Natl. Acad. Sci.* **109**, 9287–9292 (2012).
26. Zhai, D. *et al.* Highly sensitive glucose sensor based on Pt nanoparticle/polyaniline hydrogel heterostructures. *ACS Nano* **7**, 3540–3546 (2013).
27. Cornwell, D. J., Okesola, B. O. & Smith, D. K. Multidomain hybrid hydrogels: spatially resolved photopatterned synthetic nano-materials combining polymer and low molecular weight gelators. *Angew. Chem.* **126**, 12669–12673 (2014).
28. de Jong, J. J. *et al.* Light driven dynamic pattern formation. *Angew. Chem.* **44**, 2373–2376 (2005).
29. Draper, E. R., Eden, E. G., McDonald, T. O. & Adams, D. J. Spatially resolved multicomponent gels. *Nat. Chem.* **7**, 848 (2015).
30. Eastoe, J., Sánchez-Dominguez, M., Wyatt, P. & Heenan, R. K. A photo-responsive organogel. *Chem. Commun.* **14**, 2608–2609 (2004).
31. Nolan, M. C. *et al.* Optimising low molecular weight hydrogels for automated 3D printing. *Soft Mater.* **13**, 8426–8432 (2017).
32. Wei, Q. *et al.* Printable hybrid hydrogel by dual enzymatic polymerization with superactivity. *Chem. Sci.* **7**, 2748–2752 (2016).
33. Raeburn, J. *et al.* Electrochemically-triggered spatially and temporally resolved multi-component gels. *Mat. Horizons* **1**, 241–246 (2014).
34. Inostroza-Brito, K. E. *et al.* Co-assembly, spatiotemporal control and morphogenesis of a hybrid protein-peptide system. *Nat. Chem.* **7**, 897 (2015).
35. Olive, A. G. *et al.* Spatial and directional control over self-assembly using catalytic micropatterned surfaces. *Angew. Chem.* **53**, 4132–4136 (2014).
36. Rodon, F. *et al.* Localized supramolecular peptide self-assembly directed by enzyme-induced proton gradients. *Angew. Chem.* **129**, 16200–16204 (2017).
37. Hu, B. *et al.* Supramolecular hydrogels for antimicrobial therapy. *Chem. Soc. Rev.* **47**, 6917–6929 (2018).
38. Okesola, B. O. & Smith, D. K. Applying low-molecular weight supramolecular gelators in an environmental setting-self-assembled gels as smart materials for pollutant removal. *Chem. Soc. Rev.* **45**, 4226–4251 (2016).
39. Weiss, Richard G., *Molecular gels: structure and dynamics*, Monographs in supramolecular chemistry, no. 25., Cambridge: Royal Society of Chemistry (2018)
40. Bordes, R., Tropsch, J. & Holmberg, K. Counterion specificity of surfactants based on dicarboxylic amino acids. *J. Colloid Interface Sci.* **338**, 529–536 (2009).
41. Pinazo, A., Pons, R., Pérez, L. & Infante, M. R. Amino acids as raw material for biocompatible surfactants. *Ind. Eng. Chem. Res.* **50**, 4805–4817 (2011).
42. Nakata, K., Tsuchido, T. & Matsumura, Y. Antimicrobial cationic surfactant, cetyltrimethylammonium bromide, induces superoxide stress in *Escherichia coli* cells. *J. Appl. Microbiol.* **110**, 568–579 (2011).
43. Hrenovic, J. & Ivankovic, T. Toxicity of anionic and cationic surfactant to *Acinetobacter junii* in pure culture. *Open Life Sci.* **2**, 405–414 (2007).
44. Maiti, K., Bhattacharya, S. C., Moulik, S. P. & Panda, A. K. Physicochemical studies on ion-pair amphiphiles: Solution and interfacial behaviour of systems derived from sodium dodecylsulfate and n-alkyltrimethylammonium bromide homologues. *J. Chem. Sci.* **122**, 867–879 (2010).
45. Li, J.-L. & Liu, X.-Y. Microengineering of soft functional materials by controlling the fiber network formation. *J. Phys. Chem. B* **113**, 15467–15472 (2009).
46. Li, S. *et al.* Synthesis and thermoelectric properties of the new oxide materials $\text{Ca}_{3-x}\text{Bi}_x\text{Co}_9\text{O}_{19+\delta}$ ($0.0 < x < 0.75$). *Chem. Mater.* **12**, 2424–2427 (2000).
47. Herwig, P., Kayser, C. W., Müllen, K. & Spiess, H. W. Columnar mesophases of alkylated hexa-peri-hexabenzocoronenes with remarkably large phase widths. *Adv. Mater.* **8**, 510–513 (1996).
48. Aouini, A. *et al.* Chemical-physical characterization of a binary mixture of a twist bend nematic liquid crystal with a smectogen. *Curr. Comput. Aided Drug Des.* **10**, 1110 (2020).
49. Baral, M. *et al.* Interfacial and aggregation behavior of dicarboxylic amino acid based surfactants in combination with a cationic surfactant. *Langmuir* **35**, 15306–15314 (2019).
50. Maréchal, J.-P., Matsumura, K., Conlan, S. & Hellio, C. Competence and discrimination during cyprid settlement in *Amphibalanus amphitrite*. *Int. Biodeterior. Biodegrad.* **72**, 59–66 (2012).
51. van der Kooij, F. M. & Lekkerkerker, H. N. Formation of nematic liquid crystals in suspensions of hard colloidal platelets. *J. Phys. Chem. B* **102**, 7829–7832 (1998).
52. Fan, S. R., Willis, P. C. & Clark, N. A. The field induced stripe texture in surface stabilized ferroelectric liquid crystal cells. *Ferroelectrics* **121**, 127–136 (1991).
53. Kokini, J. L., Kadane, J. B. & Cussler, E. L. Liquid texture perceived in the mouth. *J. Texture Struct.* **8**, 195–218 (1977).
54. Haas, W. E. & Adams, J. E. Electrically variable diffraction in spherulitic liquid crystals. *Appl. Phys. Lett.* **25**, 263–264 (1974).
55. Bag, B. G., Hasan, S. N., Pongamorn, P. & Thasana, N. First hierarchical self-assembly of a seco-triterpenoid α -onocerin yielding supramolecular architectures. *Chem. Select* **2**, 6650–6657 (2017).
56. Criado-Gonzalez, M. *et al.* Enzyme-assisted self-assembly within a hydrogel induced by peptide diffusion. *Chem. Commun.* **55**, 1156–1159 (2019).
57. Bhattacharya, S. & Acharya, S. G. Pronounced hydrogel formation by the self-assembled aggregates of N-alkyl disaccharide amphiphiles. *Chem. Mater.* **11**, 3504–3511 (1999).
58. Datta, S. & Bhattacharya, S. Multifarious facets of sugar-derived molecular gels: molecular features, mechanisms of self-assembly and emerging applications. *Chem. Soc. Rev.* **44**, 5596–5637 (2015).
59. Piras, C., Slavik, P. & Smith, D. K. Self-assembling supramolecular hybrid hydrogel beads. *Angew. Chem.* **34**, 567–571 (2014).
60. Uva, M. & Atri, A. Surface morphology at the microscopic scale, swelling/deswelling, and the magnetic properties of PNIPAM/CMC and PNIPAM/CMC/Fe₃O₄ hydrogels. *Gels* **2**, 30–34 (2016).
61. Mukherjee, A. *et al.* Gold-catalyzed 1, 2-difunctionalizations of aminoalkynes using only N- and O-containing oxidants. *J. Am. Chem. Soc.* **133**, 15372–15375 (2011).
62. Sul, L., Wang, F. & Li, B. Adult-onset hypothyroidism impairs paired-pulse facilitation and long-term potentiation of the rat dorsal hippocampo-medial prefrontal cortex pathway in vivo. *Brain Res.* **1096**, 53–60 (2006).
63. Varughese, P., Saban, K., George, J., Paul, I. & Varghese, G. Crystallization and structural properties of calcium malonate hydrate. *J. Mater. Sci.* **39**, 6325–6331 (2004).

64. Xia, Y., Tse, C. & Lau, F.C.-M. Performance of differential chaos-shift-keying digital communication systems over a multipath fading channel with delay spread. *IEEE Trans. Circuits Syst. II Express Briefs* **51**, 680–684 (2004).
65. Weiss, I. M., Muth, C., Drumm, R. & Kirchner, H. O. Thermal decomposition of the amino acids glycine, cysteine, aspartic acid, asparagine, glutamic acid, glutamine, arginine and histidine. *BMC Biophys.* **11**, 2–7 (2018).
66. Nahak, P. *et al.* Influence of lipid core material on physicochemical characteristics of an ursolic acid-loaded nanostructured lipid carrier: An attempt to enhance anticancer activity. *Langmuir* **32**, 9816–9825 (2016).
67. Sun, M.-L. *et al.* Characterization and biotechnological potential analysis of a new exopolysaccharide from the arctic marine bacterium *Polaribacter* sp. SM1127. *Sci. Rep.* **5**, 18435–18441 (2015).
68. Jemal, A. *et al.* Cancer statistics. *CA Cancer J. Clin.* **57**, 43–66 (2007).
69. Agbaje, T., Mondal, S., Makukula, Z., Motsa, S. & Sibanda, P. A new numerical approach to MHD stagnation point flow and heat transfer towards a stretching sheet. *Ain Shams Eng. J.* **9**, 233–243 (2018).
70. Karmakar, A., Jana, D., Dutta, K., Dua, P. & Ghosh, C. Prevalence of panton-valentine leukocidin gene among community acquired *Staphylococcus aureus*: A real-time PCR study. *J. Pathog.* **2**, 245–249 (2018).
71. Dutta, K. *et al.* Benzyl isocyanate isolated from the leaves of *Psidium guajava* inhibits *Staphylococcus aureus* biofilm formation. *Biofouling* **36**, 1000–1017 (2020).
72. Karmakar, A., Dua, P. & Ghosh, C. Biochemical and molecular analysis of *Staphylococcus aureus* clinical isolates from hospitalized patients. *Can. J. Infect. Dis. Med. Microbiol.* **90**, 1636, 24–29 (2016).
73. McGuinness, W. A., Malachowa, N. & DeLeo, F. R. Vancomycin resistance in *Staphylococcus aureus*. *J. Biol. Med.* **90**, 269–281 (2017).
74. Bordes, R. & Holmberg, K. Physical chemical characteristics of dicarboxylic amino acid-based surfactants. *Colloids Surf. A* **391**, 32–41 (2011).
75. Kaler, E. W., Herrington, K. L., Murthy, A. K. & Zasadzinski, J. A. Phase behavior and structures of mixtures of anionic and cationic surfactants. *J. Phys. Chem.* **96**, 6698–6707 (1992).
76. Choffat, F. *et al.* Synthesis and characterization of linear poly (dialkylstannane). *Macromolecules* **40**, 7878–7889 (2007).
77. Sastry, N. V. & Singh, D. K. Surfactant and gelation properties of acetylsalicylate based room temperature ionic liquid in aqueous media. *Langmuir* **32**, 10000–10016 (2016).
78. Preston, K. L., Bigelow, G. E., Bickel, W. K. & Liebson, I. A. Drug discrimination in human postaddicts: Agonist-antagonist opioids. *J. Pharm. Exp. Therap.* **250**, 184–196 (1989).
79. Weichert, A. & Hoffmann, H. M. R. Synthesis and reactions of alpha-methylene-beta-keto sulfones. *J. Org. Chem.* **56**, 4098–4112 (1991).
80. du Sert, N. P. *et al.* The ARRIVE guidelines 2.0: Updated guidelines for reporting animal research. *PLOS Biol.* **18**, 3000410–3000417 (2020).
81. OECD, Test No. 404: Acute Dermal Irritation/Corrosion. OECD Publishing, Paris (2002)
82. Sufian, A. & Russell, A. R. Microstructural pore changes and energy dissipation in Gosford sandstone during pre-failure loading using X-ray CT. *Int. J. Rock Mech. Min. Sci.* **57**, 119–131 (2013).
83. Biswas, S. *et al.* Quorum sensing auto inducer (s) and flagellum independently mediate EPS signaling in *Vibrio cholerae* through luxO-independent mechanism. *Microbiol. Ecol.* **77**, 616–630 (2019).

Acknowledgements

This work has been financially supported by University Grants Commission (UGC), New Delhi, India through a UGC-BSR Scheme, (F.25-1/2014-15(BSR)/7-234/2009(BSR) UGC-SAP (No. F. 5-9/2015/DRS-II (SAP-II) and Department of Science and Technology, Govt. of India, New Delhi, India through the DST-FIST grants (No. SR/FST/CS-1/2017/7 (C).

Author contributions

MB, EM, HS and MKM studied the physicochemical properties KCG, TM and CG studied the biological activities AP and AL synthesized the anionic surfactants PM studied the DSC and TGDTA CC, CG, AKP and SB prepared the manuscript.

Competing interests

The authors declare no competing interests.

Additional information

Supplementary Information The online version contains supplementary material available at <https://doi.org/10.1038/s41598-021-94777-2>.

Correspondence and requests for materials should be addressed to A.K.P.

Reprints and permissions information is available at www.nature.com/reprints.

Publisher's note Springer Nature remains neutral with regard to jurisdictional claims in published maps and institutional affiliations.



Open Access This article is licensed under a Creative Commons Attribution 4.0 International License, which permits use, sharing, adaptation, distribution and reproduction in any medium or format, as long as you give appropriate credit to the original author(s) and the source, provide a link to the Creative Commons licence, and indicate if changes were made. The images or other third party material in this article are included in the article's Creative Commons licence, unless indicated otherwise in a credit line to the material. If material is not included in the article's Creative Commons licence and your intended use is not permitted by statutory regulation or exceeds the permitted use, you will need to obtain permission directly from the copyright holder. To view a copy of this licence, visit <http://creativecommons.org/licenses/by/4.0/>.

© The Author(s) 2021